The Optics of Turbulent Compressible Vortices

RAHUL RAMPAL

A Thesis

In The Department

Of

Mechanical Engineering

Presented in Partial Fulfillment of the Requirements

for the Degree of Master of Applied Science (Mechanical Engineering)

at Concordia University

Montreal, Quebec, Canada

June 2014

Concordia University

School of Graduate Studies

This is to certify that the thesis prepared

By: RAHUL RAMPAL

Entitled: The Optics of Turbulent Compressible Vortices

and submitted in partial fulfillment of the requirements for the degree of

Master of Applied Science in Mechanical Engineering

Complies with regulations of the University and meets the accepted standards with respect to originality and quality.

Signed by the final examining committee:

Dr. Mingyuan Chen	Chair
Dr. Wahid S. Ghaly	Examiner
Dr. Andreas K. Athienitis	Examiner
Dr. Georgios. H. Vatistas	Supervisor

Approved By: Chair of Department or Graduate Program Director

Dean of Faculty

Date June 30th, 2014

Abstract

The optics of turbulent compressible vortices

Rahul Rampal

In the past, a few investigators have examined theoretically and experimentally the optical properties of laminar compressible vortices. However, there is no theoretical study found in the scientific or technical literature for the turbulent kind. This thesis deals with the refracted shadows produced by turbulent compressible vortices. The construction of the theory is accomplished extending the previous laminar approach to include the effects of turbulence.

The pressure, temperature and density are calculated solving numerically the conservation of mass, momentum and energy equations along with the equation of state for the case of a turbulent vortex evolving in a compressible, viscous, heat conducting and calorically perfect gas in an unconfined domain. The radial distribution of light intensity is then deduced using the past general mathematical relation that links the density to luminosity of the shadowgraphs casted on an image plane by light ray refraction.

The differences in luminosity of laminar and turbulent vortices with Mach numbers ranging from 0.4 to 0.8 are compared. The darkness of the central disc and luminosity of the bright ring are found to be a function of the vortex Mach number: the higher the Mach number, the darker the disks and the brighter are the halos. Vortices of the turbulent kind are found to produce different shadow signatures than the laminar. Alike to the laminar case and depending on the focal length, turbulent vortices can also generate the previously disputed two caustics. The

last effect is shown to generate the combination of dark circular area near the vortex center, followed by a thin halo that is succeeded by a dim ring, which is subsequently followed by a thicker corona.

In the future, the present methodology can potentially be developed to recover the thermo-fluid properties optically.

Keywords: Vortex model, compressible vortices, turbulent vortices, optics of vortices, shadowgraphy.

Acknowledgements

Foremost, I would like to express my sincere gratitude to my supervisor Dr. Georgios H. Vatistas for his continuous support and financial help during my Masters study and research. He has guided me with motivation, enthusiasm and immense knowledge during my research and thesis writing. I have been benefited not only in the studies but also in life with his wide knowledge and life experience. I could not have imagined having a better advisor and mentor.

I am also deeply grateful to my father for his all kind of support. I would also like to thank my sisters, Reena and Manu, for their emotional support and their valuable suggestions. I would like to dedicate this thesis to

"My loving mother, Prem Lata"

Table of Contents

List of figures

List of Tables

Nomenclature

C	Constant	m^3/kg
c_p, c_v	heat capacities constant pressure and constant volume	W s/kg K
E	Light intensity	lm/m^2
H	Normalized axial velocity component	β Re h
k	Thermal conductivity	W/m K
l	Distance from the test section to image plane	m
p	Static pressure	Pa
q	Total velocity vector	m/s
R	Gas constant	J/kg K
r, z	Radial and Axial coordinates	m
θ	Azimuthal coordinate	radian
r_c	Core radius	m
r_d	Central dark disk radius	m
T	Static temperature	K
U	Normalized radial velocity component	β Re u
V	Normalized tangential velocity component	m/s
V_r, V_θ, V_z	Radial, Tangential and Axial velocity component	m/s
$V_{\theta c}$	Core tangential velocity	$\Gamma_\infty/2\,\pi\,r_c$
x,y	Cartesian coordiantes	m

Dimensionless characters

a	Scaling constant	
c_0, c_1	dimensionless general constants	
L	Large dimensionless number	
m	constant for turbulent flow, (a+1)/4	
M_0	Vortex Mach number	$V_\theta/\sqrt{(\gamma\ R\ T_\infty)}$
n	Vortex exponent of the n- family	
O	Order of magnitude	
Pr	Prandtl number	$\mu\ c_p/k$
Re	Vortex reynold number	$\rho_\infty . V_{\theta c} .\ r_c/\mu$
u	Dimensionless radial velocity component	$V_r/V_{\theta c}$
v	Dimensionless tangential velocity component	$V_\theta/V_{\theta c}$
w	Dimensionless axial velocity component	$V_z/V_{\theta c} = zh$
x, X	Dimensionless dummy variables	

Greek characters

α	Angle of refraction	radian
Γ_∞	Vortex circulation	m^2/s
$\delta\alpha$	Finite change of angle of refraction	radian
δy	Finite change in the y-direction	m
μ	Fluid viscosity	kg/m s
ρ	Fluid density	kg/m^3

σ	Lumped parameters	$\rho_\infty C$
Φ	Viscous dissipation function	W/m^3

Dimensionless Greek characters

β	Dimensionless density	ρ/ρ_∞
γ	Specific heat ratio	c_p/c_v
Θ	Dimensionless static temperature	T/T_∞
κ	Dimensionless Constant	
λ	Dimensionless distance from test section to image plane	l/r_c
ξ,ζ	Dimensionless coordinates	r/r_c and z/r_c
δ	Dimensionless small number	
η	Refractive index	
Σ	Dimensionless light intensity	
Π	Dimensionless static pressure	$p/\rho_\infty V_{\theta c}^2$

Subscripts

im pl	Image plane
∞	Infinity
1,2	Optical stations 1 and 2
c	Core
d	dark disk boundary

Chapter 1. Introduction

1.1. General

Although the scientific study of vortices begun in the Victorian era, the study on vortex optics started relatively late. Berry and Hajnal (1983) published a study on the visual properties of solid bodies such as spheres floating in slightly deformed water surfaces. Based on the principle of caustics, they also examined the shadows casted by a decaying free-vortex. Sterling et al. (1987) driven by curiosity investigated the appearance of dark disks surrounded by bright rings at the bottom of a swimming pool when the free-water vortex surface is uniformly illuminated from above. This strange manifestation was noticed first in March of 1986, by the last author (see Fig. 1.1). They also identified the cause of the shadowy disk-bright/halo combination in images using Snell's law and employed different free-surface profiles generated by various types of vortices. The theoretical surface of revolution profiles that they explored were: parabolic, hyperbolic, and finally their combination.

Figure 1.1. The shadows casted at the bottom of a swimming pool by vortices (Kiehn, 1987).

Two systems are analogous, if they are described by similar sets of dimensionless equations. A well-known example of flow fields of this kind is the likeness of free-surface shallow water hydraulics and the two-dimensional compressible gas flows (Landau & Lifshitz, 1987). According to this similitude, the perturbation in liquid elevations in open channel flow corresponds to the gas density variations in a compressible flow. Although this analogy is not rigorous (Thompson, 1972), shallow water experiments have been routinely used to qualitatively describe compressible gas flows.

There are a number of ways that one can use to identify and study compressible vortices. Shadowgraphy (the study of shadows) is a simple method to visualize these vortices. The technique uses the fact that the value of the refractive index depends on the density of

homogenous transparent media. Since, the speed of light in gases is only marginally different than that in empty space, the Gladstone-Dale relation:

$$\left(\frac{\eta - 1}{\rho}\right) = C \qquad \ldots \quad (1.1)$$

estimates reasonably dilute gases (Liepmann & Roshko, 1957).

When the gas density varies at a section, light rays passing through it will refract, thus casting a shadowy picture on the image plane. In reverse, one can obtain in theory, the density variation from the shadow-light intensity signature. The other basic properties can then be recovered using an appropriate vortex model.

There have been a relatively decent number of contributions on the visualization of compressible blade vortices in the helicopter aerodynamics community. Heavily loaded helicopter blades produce compressible eddies that when illuminated, due to the changes in refractive index, become visible. Parthasarathy et al. (1987), Norman and Light (1986) and Swanson and Light (1992) attempted to relate the fundamental properties of tip vortices in helicopter blades using wide field shadowgraphy.

The likeness between gaseous and liquid vortices can be seen vividly in the shadow images of Parthasarathy et al. (1987), Swanson and Light (1992) and Sterling et al. (1987). The last similar appearance is, of course, due to the previously mentioned origin in which the refraction index depends on the density distribution of gas and the free surface elevation curvature in liquids. Comparable shadowgraphs, due to the liquid/gas analogy, disclosing clearly the presence of an assortment of vortices in a liquid, generated in the wakes of a translating

wooden plank and in a supersonic stream behind a triangular wedge are shown in Figs. 1.2 (a) and (b), respectively.

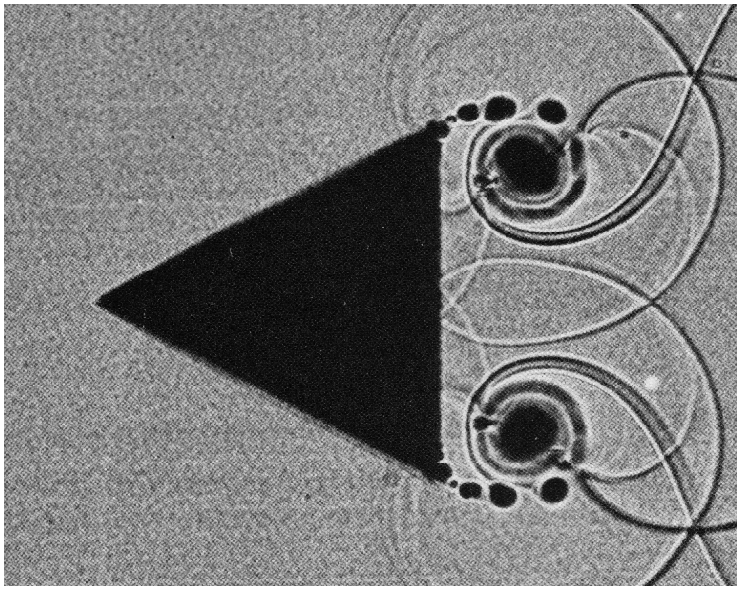

(a)

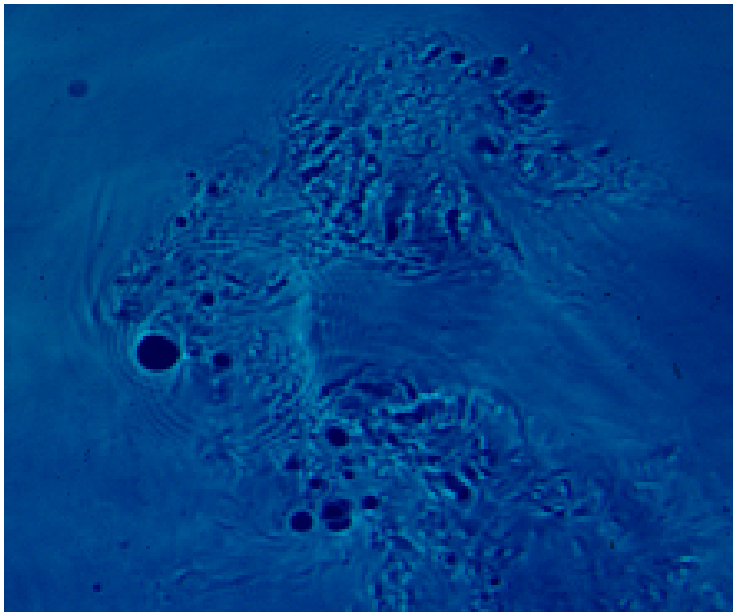

(b)

Figure 1.2. (a) Vortices in the supersonic wake behind a triangular wedge identifiable with the dark disk/bright rings (Van Dyke, 1982). (b) Similar vortex patterns were produced at the bottom of a swimming pool generated using a thin wooden plank by Vatistas and Abderrahmane (2008).

Bagai and Leishman (1993) derived a mathematical relation for direct shadowgraphs and Schlieren contrast variation. They established that the differences in contrast are sensitive to the overall vortex profile as well as the location of peak peripheral velocity. Vatistas (2006a) studied the refracted shadows of a $n = 2$ laminar compressible vortices. He allowed the flow to transfer heat and dissipate mechanical energy instead of being isentropic. Porter (2011) examined the optical environment of helicopter tip vortices in both near and far field under different flight conditions using various techniques including shadowgraphy.

Recent work has shown that the general topic could also be of interest in solar physics (Vatistas, 2011). The dark disk shape appearance in the central part of sunspots is traditionally attributed to a sort of cooling effect (due to an unidentified cause) experienced by the ionized gas. However, the last cannot justify at the same time the bright ring-like corona (see Fig. 1.3 (a)) or even worst the second dimmed ring followed by an additional bright ring (see Fig. 1.3 (b)). An alternate explanation that can account at the same time for all of these effects is based on light refraction due to density variations in a compressible solar plasma whirl in Heliosphere (Vatistas, 2011).

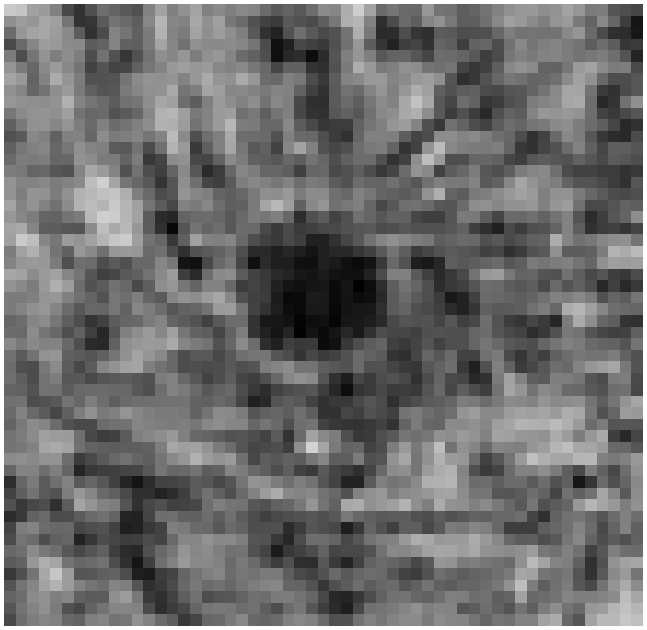

(a)

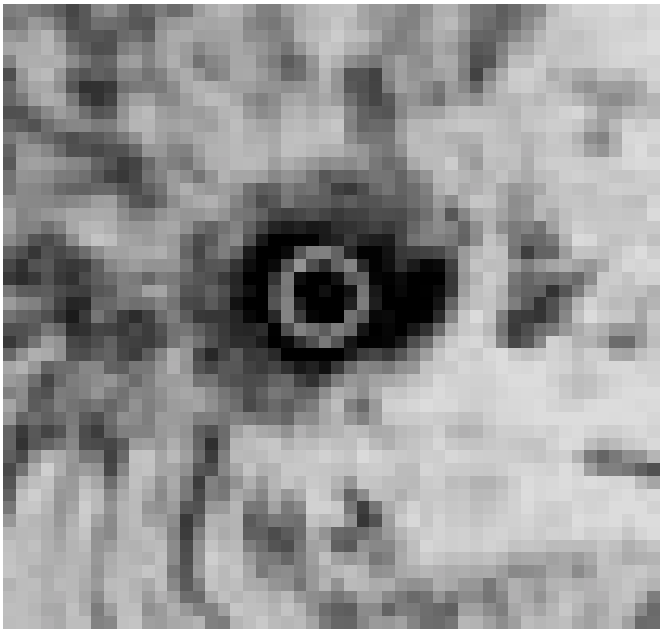

(b)

Figure 1.3. (a) Heliograph image of a sunspot showing a single dark disk/bright ring combination (Hale, 1924). (b) Sunspot image for a double combination of disks followed by halos (Hale, 2006).

Although the first experiments of Sterling et al. (1987) were performed illuminating the liquid vortices from above, recent test made in our laboratory have indicated that the same shadow will be generated if illumination is made from below (see Fig. 1.4). The last is an essential piece of information since the light produced in the Heliosphere, due to thermonuclear hydrogen fusion, produces photons that emanate outwards from the solar surface. By analogy, the same shadow signature will be obtained if a compressible vortex is illuminated from either side.

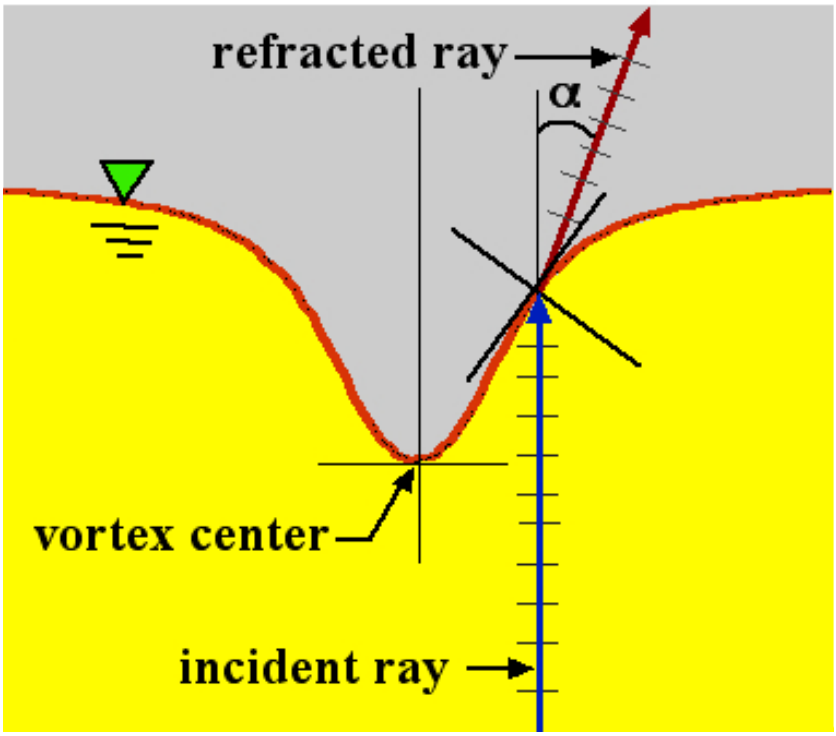

(a)

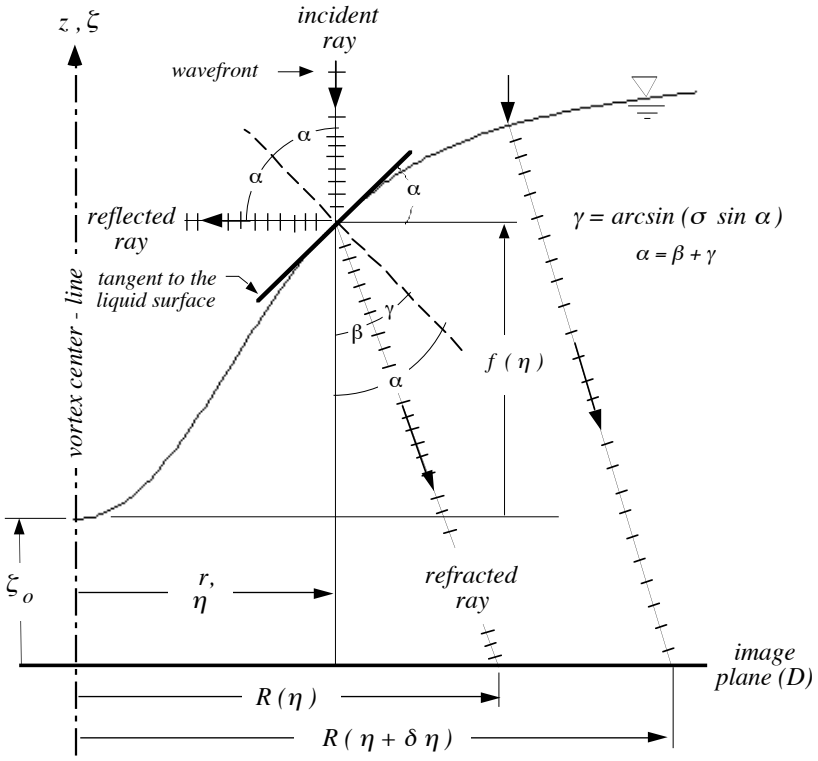

(b)

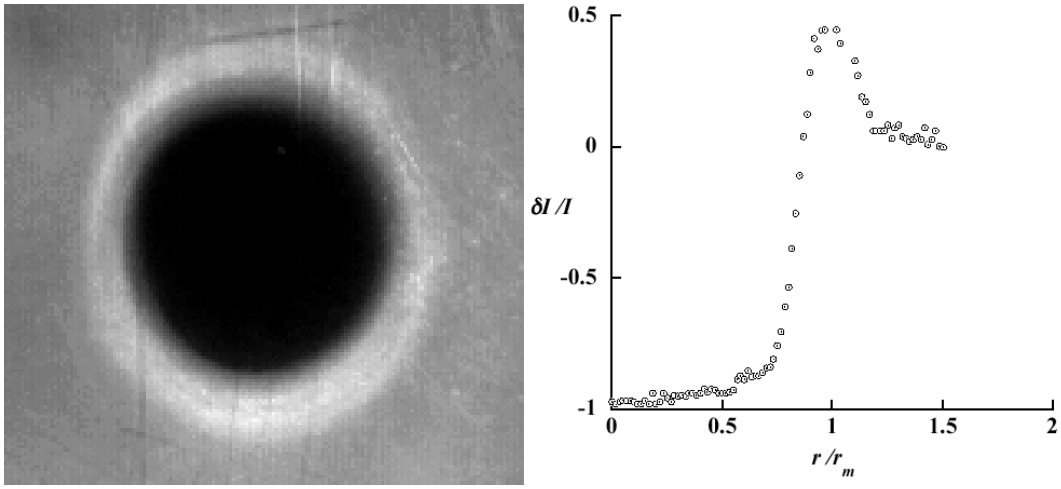

(c) (d)

Figure 1.4. (a) Refraction of light in a liquid vortex with an interface while illuminating the whirl from below (Vatistas, 2011). (b) Refraction of light in a liquid vortex with an interface

while illuminating the whirl from above. (Aboelkassem & Vatistas, 2007). (c) Actual shadowgraph of a liquid vortex photographed recently in our laboratory, generated towing a flat ruler in a water tank (Vatistas, 2011). (d) The radial profile of light intensity obtained from the digitized image (Vatistas, 2011).

1.2. Thesis objectives

In this thesis, taking advantage of the recent advances in the characterization of vortices (Vatistas & Badwal, April 2014, March, 2014)**,** the optics of turbulent compressible heat conducting whirls is now examined numerically. Comparison between the laminar and turbulent compressible vortices will be made using numerical shadowgraphy. Different focal lengths are used to study their effect on the shadows casted in the image plane.

The main objectives of this thesis are:

- Simulate the shadows generated by turbulent gaseous vortices, considering a heat-conducting medium of large extend.
- Obtain numerically the radial distribution of the refracted light intensity of these vortices.
- Examine the effect that Mach number and focal length have on the light intensity profile.
- Compare the differences of intensity distributions between turbulent and laminar compressible vortices under the same conditions.

Chapter 2. Literature Review

2.1. Introduction to vortices

Vortices are important forms of fluid motion that have their origin on the type of rotation that elementary fluid element undergo. In the words of Saffman and Baker (1979), considering the original form of a vortex proposed by Rankine:

"A vortex is a finite volume of rotational fluid, bounded by irrotational fluid or solid walls."

Vortices found in nature and engineering, have different sizes, shapes and strengths. They can be as small as a tiny turbulent eddy (10^{-4} m) to as large as planetary vortices (10^{10} m). Common examples of this type of fluid motion include bathtub vortices, tornadoes, waterspouts, hurricanes, airplanes' trailing vortices, whirls in gas turbines and the red spot in Jupiter atmosphere.

In order to realize the intended goal, engineers have previously exploited the advantageous properties of vortices. Various industrial applications like vortex tubes, heat exchangers, separators and vortex combustors etc. are prime examples where the vortex is necessary for the proper operation of the equipment. However, in some other applications, the presence of vortices could be highly undesirable. A representative paradigm of the unwanted effect is the wingtip vortices where the induced drag caused by them, counteracts the thrust and thus, decreases the wings' lifting efficiency. The presence of these strong whirls produce also

vibrations and noise. These have been the main reasons as to why engineers have tried hard to reduce or even eliminate their adverse contributions.

Vorticity is the fluid property that characterizes the rotation of the elementary fluid elements. Depending on their vorticity value, these are classified as either free or forced vortices. In a free vortex, the curl (or vorticity) of the velocity vector field is zero, fluid elements as they move, do not rotate about their own axes and as such this type of eddies are also referred to as irrotational. Since, under this condition, a velocity potential exists they are also known as potential. In a forced vortex, the curl of velocity field is non-zero (vorticity is not null) and thus, these are rotational vortices.

If the tangential velocity in a vortex is considerably larger than the radial and axial components, these are classified as strong or intense vortices. In addition, if most of their vorticity exist within the central region (the core), these are identified as concentrated.

2.2. Vortex models

Vortices are considered as one of the most cumbersome subjects in fluid dynamics. There had been a number of attempts to explain and analytically represent them through mathematical models. Rankine (1858) and Helmholtz (1858) gave separately mathematical description of vortex motion that are now considered as the first step towards the scientific description of vortices. Helmholtz (1858) presented his three celebrated theorems on vorticity. Rankine (1858) proposed a model, which related the tangential velocity to the radius. This model assumes a

forced vortex to exist within the core $\left(r \le r_c\right)$ followed by a potential vortex outside the core $\left(r \ge r_c\right)$.

As is the case with any original attempt, Rankine's simple archetype has several problems. The radial and axial velocity components are zero. Furthermore, there is a jump discontinuity for the vorticity at the point of transition (r_c, core radius) and the theoretical tangential velocity overestimates the actual.

Burgers (1948) improved Rankine's model to better correlate the experimental results. Unfortunately, in Burgers representation of real vortices, the radial velocity is unbounded in the radial direction and as such it is not suitable for unconfined vortices. The previous formulations pertained to one cell flow configuration in the radial-axial plane (see Fig. 2.1(a)).

Sullivan (1959) proposed an alternate two-cell vortex model (Fig. 2.1.(b)), that have the same physical impediments of problem as Burgers (1948).

Vatistas et al. (1991) came up with a vortex formulation presently known as Vatistas vortex model. The model has a constant '*n*' that can only assume values greater than 1. Subsequently, Vatistas and his team advanced the original model (Vatistas, 1998, 2006b; Vatistas & Aboelkassem, 2006a, 2006b; Vatistas et al., 2005) that can better explain the physics of decaying vortices.

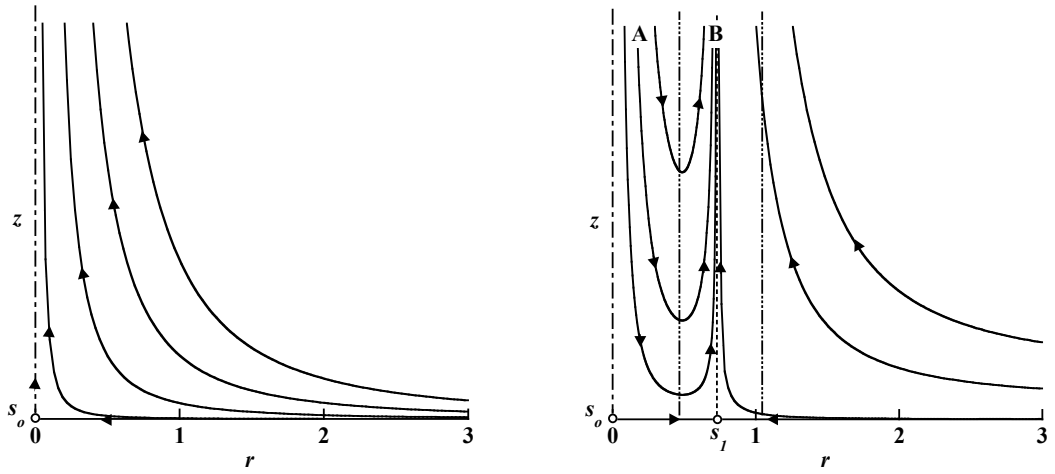

(a) (b)

Figure 2.1. Flow pattern structure in the *r-z* plane for (a) one- and (b) two-cell vortices. (Credits: G.H. Vatistas)

Some of the most known and heavily used incompressible steady vortex models are discussed next in more detail.

2.2.1. The Rankine model

Rankine (1858) proposed the simplest of the vortex models. He neglected both radial and axial velocity components and hypothesized that the tangential velocity component was only a function of the radius. His formulation assumed a linear distribution of tangential velocity inside the core and hyperbolic variation outside the core i.e. he assumed a forced vortex inside the core and free vortex outside. Mathematically,

$$V \propto \begin{cases} \xi \quad for \quad \xi < 1 \\ 1/\xi \quad for \quad \xi \geq 1 \end{cases} \qquad \ldots(2.1)$$

$$\text{And } U = W = 0 \qquad \ldots(2.2)$$

This model approximates reasonably the experimental tangential velocity distribution except in the neighborhood of the core. The static pressure correlation with the observed values is also reasonable (Vatistas, 1998) which indicates that non-conformities of velocity with the experiment near $\xi = 1$ does not influence the pressure in a drastic way. The last velocity profile, however, produces a jump discontinuity at core for the associated vorticity, which together with the absence of radial and axial velocity components makes this model unrealistic.

2.2.2. The Burgers model

Burgers (1948) proposed a model that provides for a smooth transition of the tangential velocity near the core, assuming a linear radial velocity distribution.

$$U = -\frac{2\kappa}{\mathrm{Re}}\xi \qquad \ldots(2.3)$$

Using the above radial velocity, the tangential and axial velocity components are found from the θ-momentum and continuity equations, respectively:

$$V = \frac{1}{\xi}\left\{1 - \exp\left(-\kappa\xi^2\right)\right\} \qquad \ldots(2.4)$$

$$W = \frac{4\kappa}{\mathrm{Re}.\zeta} \qquad \ldots(2.5)$$

This model, however, has serious limitation that the radial velocity becomes infinite when ξ approaches infinity. The last makes the formulation inapplicable to unconfined vortices without some further drastic simplifications.

2.2.3. The Vatistas model

Vatistas et al. (1991) formulated a new vortex model that assumes the following tangential velocity component.

$$V = \frac{\xi}{(1+\xi^{2n})^{(1/n)}} \qquad \ldots(2.6)$$

The above assumption was based on the work on concentrated vortices in vortex chambers where the azimuthal velocity component does not depend strongly on axial direction (Vatistas et al., 1986). Based on Eq. (2.6), the radial velocity component is then deducted from the θ-momentum equation.

$$U = \frac{-2(n+1)}{\mathrm{Re}} \frac{\xi^{(2n-1)}}{(1+\xi^{2n})} \qquad \ldots(2.7)$$

From continuity equation and Eq. (2.7), the axial velocity component is given by

$$W = \frac{4n(n+1)}{\mathrm{Re}.\zeta} \frac{\xi^{2(n-1)}}{(1+\xi^{2n})^2} \qquad \ldots(2.8)$$

For n =1, it represents Scully's (Scully, 1975) model while $n \to \infty$, it represents Rankine's (1858) model. For n = 2, the tangential velocity profile comes very close to Burgers (1948). Because of its simplicity and non-contradictory nature, it has been widely used by a number of scientist and engineers around the world.

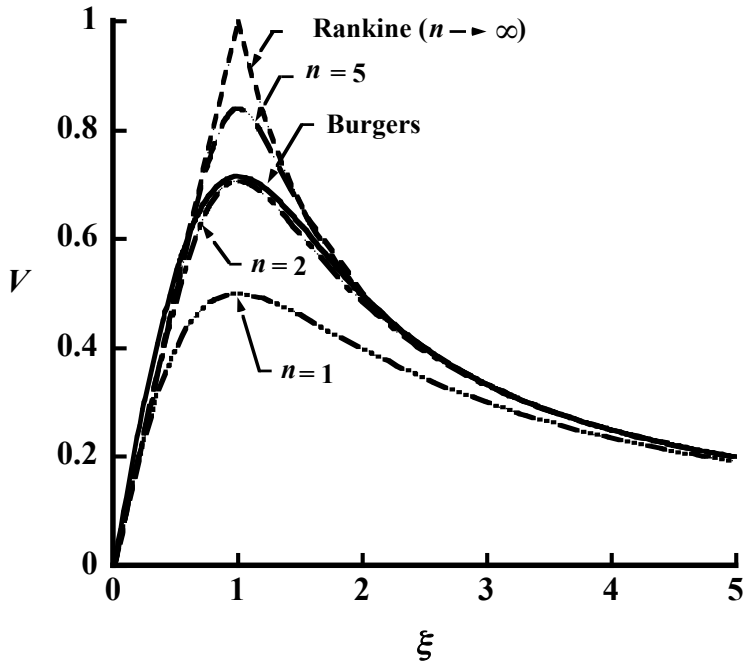

Figure 2.2. Tangential velocity for *n*-vortex profiles for different values of *n* (Vatistas et al., 1991). Depending on the choice of *n*, the velocity can assume profiles ranging from Rankine ($n \rightarrow \infty$) to Scully ($n = 1$).

Vatistas (1998) suggested yet another model for self-similar intense vortices. This model can represent single- or double-celled intense vortices. He also showed that depending upon a scaling constant, the axial velocity component could have profiles ranging from jet-like to wake-likes. In 2006, Vatistas and Aboelkassem (2006a) extended the previous work into compressible vortices. This model was used as a base to study the optical characteristics of intense vortices with the help of shadowgraphy. The density variation was achieved via the solution of the energy and state equations.

Ramasamy and Leishman (2006) investigated turbulent helicopter blade tip vortices. They found that inside the core, the flow behaves as if it was laminar. There was a flow transition to turbulent conditions when a critical Reynolds number was reached. In turbulent

vortices, the tangential velocity outside the core was seen to change at slower pace than laminar case.

Vatistas (2006b) proposed further a model, which included the effect of turbulence in tip vortices. The value of the new exponent, in the proposed tangential velocity component, was obtained by fitting the new velocity formulation to the experimental data using the least square method. Recently, Badwal (2014) combined the work of Vatistas and Aboelkassem (2006a) and Vatistas (2006b) to produce a formulation that is applicable to turbulent compressible vortices. This model is used in this thesis to study the optics of turbulent compressible vortices.

2.3. Optical Method: Shadowgraphy

The structure of vortices has been studied in the past using a number of experimental methods. Hot wire anemometry and multi-hole pitot-probes were used by Chigier and Corsiglia (1971) and Dosanjh et al. (1962), respectively. These are intrusive measuring methods that can disturb the flow and thus altering its structure. The Laser Doppler anemometry (LDA) and particle image Velocimetry (PIV) are not effective in resolving the velocity near the axis of rotation for the following reason. Inside the core, the high tangential velocity produces a finite centrifugal force that acts as a natural separator displacing the seed particles away and thus, creating a void.

Optical density gradient methods like shadowgraphy have the advantage of being completely non-intrusive i.e. it do not disturb the flow. In addition, they do not require seed

particles to function. However, these are limited by the fundamental requirement that the flow field must be compressible.

In principle, shadowgraphy (Merzkirch, 1974) does not require any optical component other than a light source and a recording plane (screen) onto which the shadow is projected (see Fig. 2.3). Due to light refraction, a shadow is generated on the image plane, its picture is recorded with a high-resolution digital camera and then, the recorded light intensity field is analyzed using the computer.

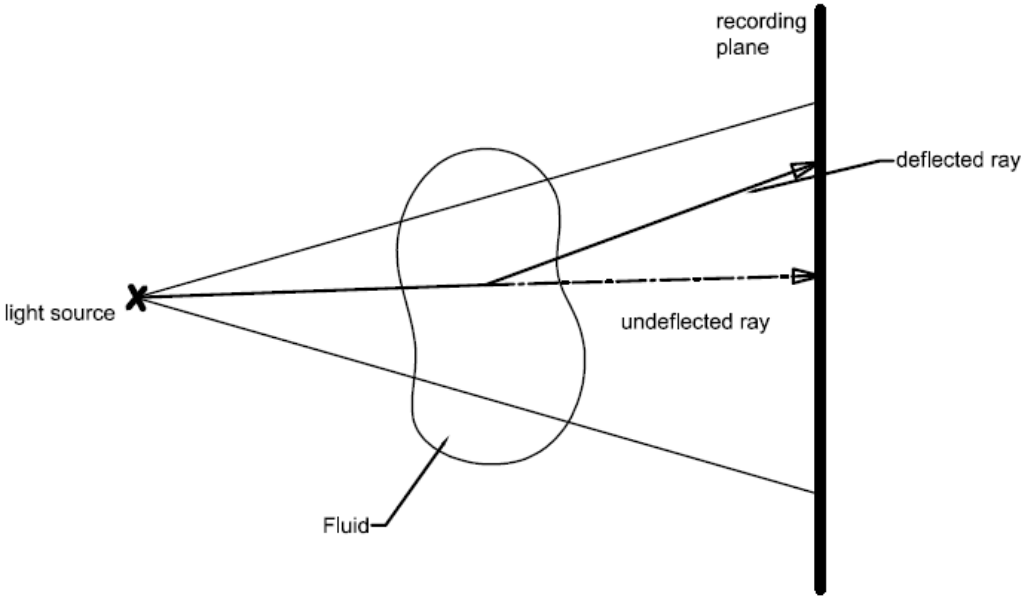

Figure 2.3. Simple setup example of Shadowgraph without optical components (Merzkirch, 1974).

2.4. Vortex optics

As discussed in chapter 1, Berry and Hajnal (1983) were among the first who initiated the work of studying vortices using the method of shadowgraphy. They studied analytically the

optical effects of deformed water surfaces by the principle of caustics. They supported their theory via three different examples: a straight floating edge, a small sphere and a dissipated free vortex.

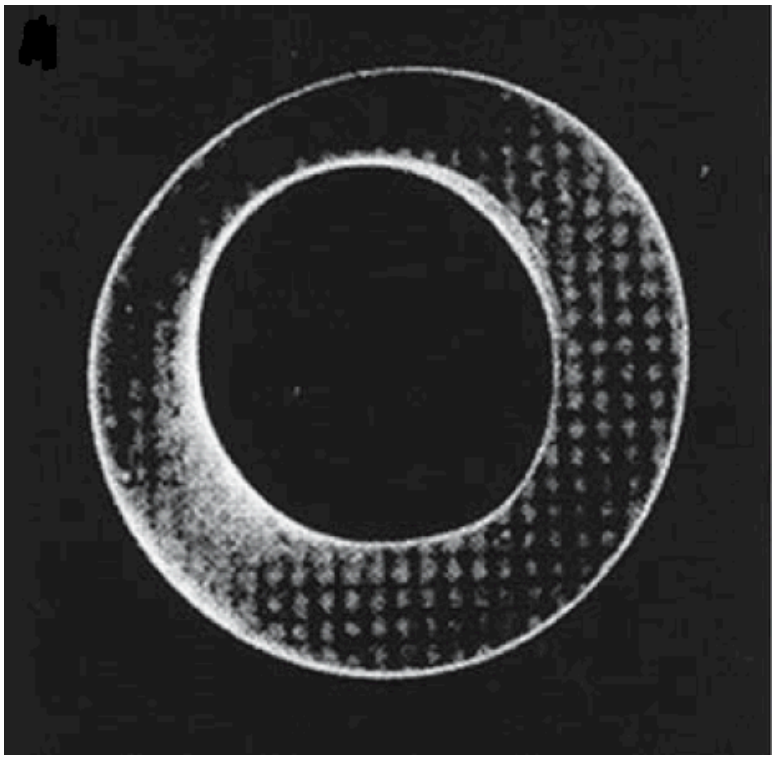

Figure 2.4. Experimentally obtained shadowgraphs of a decaying vortex showing two caustics (Berry & Hajnal, 1983).

The caustic of the free vortex consisted of two roughly cylindrical sheets that join at a cusp-edged ring. They verified their results via experiments that dealt with the shadows obtained by a floating sphere and a decaying vortex. It was found that bright-edged caustic shadows occur only when a floating object depresses the water surface. If surface is raised, it acts as a diverging lens and hence, there are no real caustics. On one hand, when water is depressed, the shadow is consistently larger than that which would have resulted if the water surface were flat. On the

other hand, when surface was raised, the shadow was smaller. One of their main conclusions was also that the shadow patterns change with the wavelength and cannot be related by scaling.

Sterling et al. (1987) provided an explanation as why the disks in liquid vortices are dark. They used Snell's law to calculate the intensity distribution in the terms of radial distance and surface of revolution by considering Rankine vortex. They also explained the qualitative nature of intensity distribution for the specific surface profiles considering three surfaces of revolution. They concluded that the diameter of the dark disk ends where the bright ring appears, while the bright ring begins where the curvature of the free surface becomes negative.

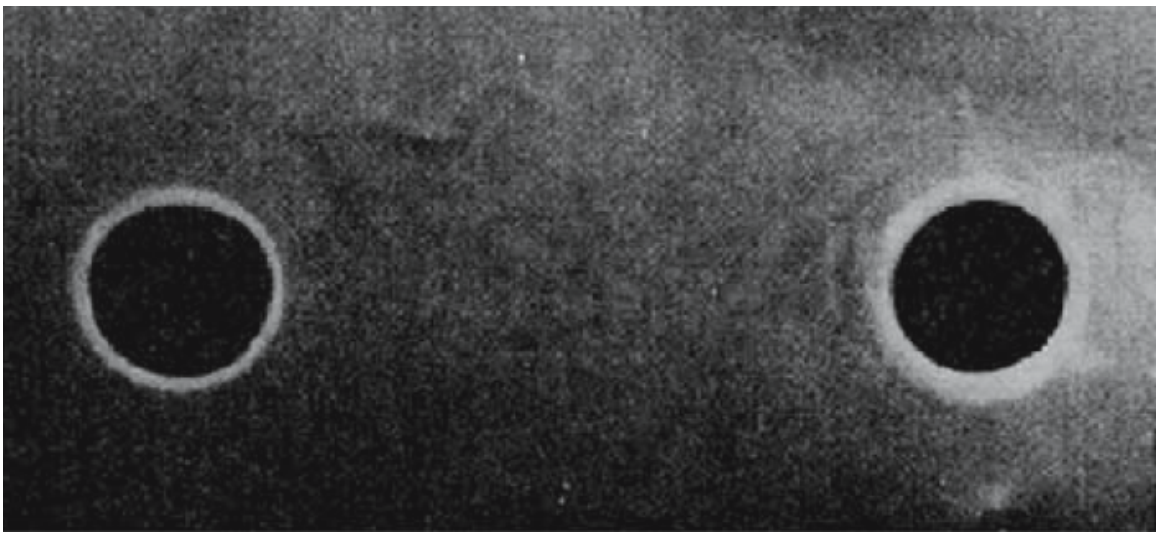

Figure 2.5. Shadowgraph of the dark-disk/halo appearance in a pair of vortices (Sterling et al., 1987).

It was also found convenient to study the rotor-generated flow-field in helicopters using shadowgraphy. Consequently, this technique became very popular in the helicopter community. Parthasarathy et al. (1987) visualized the trajectory and wake generated by helicopter blade tip vortices. They studied the effects of Mach number and angle of attack on the visibility of

vortices using this technique and concluded that it is feasible to use it in the study of flow fields generated by large main rotor either in a full-scale test or in a wind tunnel. The previous authors were also able to find the threshold value for S, which is a measure of visibility of shadowgraphs.

Norman and Light (1986) used wide field shadowgraphy to formulate contrast variation for two-dimensional vortex by assuming a small thermodynamic disturbance and also established a relationship between this contrast and the tangential velocity profile. But they could not ascertain the sensitivity of the results on either of thermodynamic approximation or other vortex models.

Swanson and Light (1992) used the method to acquire quantitative data for an isolated tilt-rotor and wing in hover. Depending upon the thrust condition and wake age, the vortex core structure was examined. They provided comparisons between tilt-rotor and helicopter rotor wake geometry measurements and also proposed improvements in the existing prescribed-wake and free-wake models.

Light et al. (1992) studied the applications of wide field technique to rotor wakes visualization and examined its feasibility for visualizing the wake of a small scale helicopter rotor in forward flight. They demonstrated that shadowgraphs could be used to obtain both qualitative and quantitative descriptions of the wake geometry, wake/body interactions and blade/vortex interactions in forward flight.

Bagai and Leishman (1993) used shadowgraphy and Schlieren methods to visualize vortex flows. They derived a relationship between contrast and velocity profiles of these two methods by assuming the homentropic flow. They also compared their derived shadowgraph

contrast with actual one to elaborate on the vortex structure, its extent and growth of viscous core. In addition, they showed that the dimensions of dark nucleus/bright ring of vortex are not, in general, equal to the dimensions of viscous vortex core.

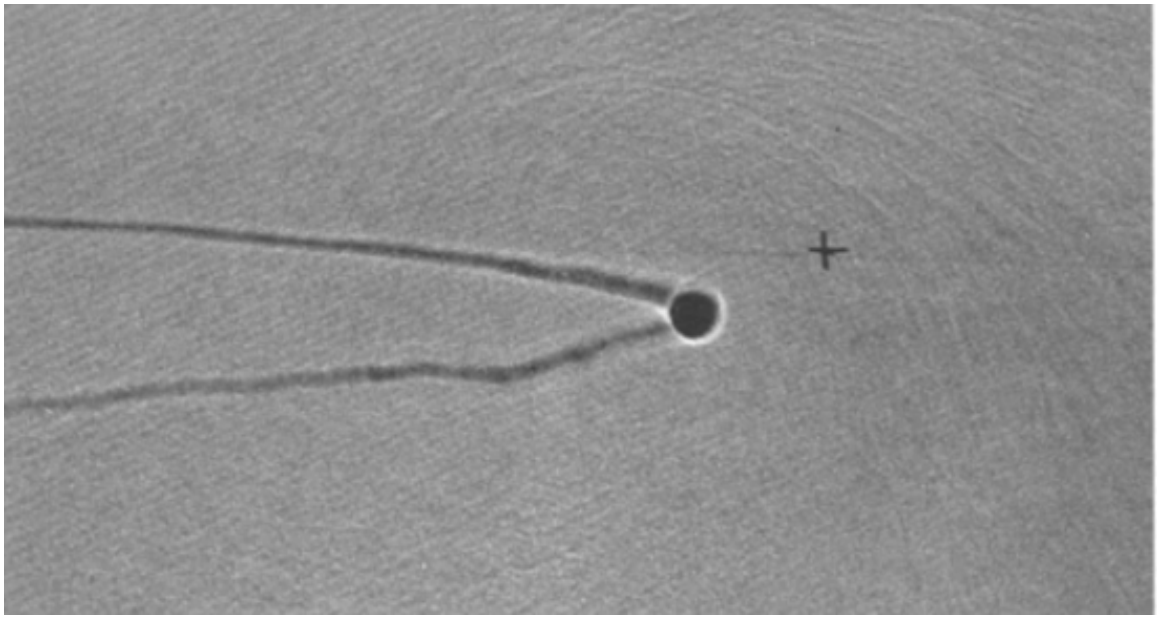

Figure 2.6. Shadow image of compressible rotor tip vortex (Bagai & Leishman, 1993).

Vatistas (2006a) studied the refracted images of vortices using a more realistic thermodynamic approximation which allowed the flow to transfer heat and dissipate mechanical energy. He also compared his shadowgraphs of laminar vortices with the ones of the vortex flow that used the isentropic approximation and provided an explanation behind the alternating dark and bright circular bands. Porter (2011) studied the aero-optical aberrations related with turbulent compressible flow fields. He used shadowgraphy to study the aero-optics effects on near and far field.

Chapter 3. Mathematical formulation

3.1. The Governing equations

The basic equations that are used to represent the problem are the conservation of mass (continuity), momentum (Navier-Stokes) and energy equations, along with the equation of state for a steady, axisymmetric and compressible flow of a calorically perfect gas.

Conservation of mass:

$$\frac{\partial(\rho V_r)}{\partial r}+\frac{\partial(\rho V_z)}{\partial z}+\frac{\rho V_r}{r}=0 \qquad \ldots(3.1)$$

Radial momentum:

$$\left(V_r\frac{\partial V_r}{\partial r}-\frac{V_\theta^2}{r}\right)=-\frac{1}{\rho}\frac{\partial p}{\partial r}+\frac{\mu}{\rho}\left(\frac{\partial^2 V_r}{\partial r^2}+\frac{1}{r}\frac{\partial V_r}{\partial r}-\frac{V_r}{r^2}+\frac{1}{3}\frac{\partial}{\partial r}\left(\frac{\partial V_r}{\partial r}+\frac{\partial V_z}{\partial z}+\frac{V_r}{r}\right)\right) \qquad \ldots(3.2)$$

Tangential momentum:

$$\left(V_r\frac{\partial V_\theta}{\partial r}+\frac{V_r V_\theta}{r}\right)=\frac{\mu}{\rho}\left(\frac{\partial^2 V_\theta}{\partial r^2}+\frac{1}{r}\frac{\partial V_\theta}{\partial r}-\frac{V_\theta}{r^2}\right) \qquad \ldots(3.3)$$

Axial momentum:

$$\left(V_r\frac{\partial V_z}{\partial r}+V_z\frac{\partial V_z}{\partial z}\right)=-\frac{1}{\rho}\frac{\partial p}{\partial z}+\frac{\mu}{\rho}\left(\frac{\partial^2 V_z}{\partial r^2}+\frac{1}{r}\frac{\partial V_z}{\partial r}+\frac{\partial^2 V_z}{\partial z^2}+\frac{1}{3}\frac{\partial}{\partial z}\left(\frac{\partial V_r}{\partial r}+\frac{\partial V_z}{\partial z}+\frac{V_r}{r}\right)\right) \qquad \ldots(3.4)$$

Energy:

$$\frac{k}{r}\frac{d}{dr}\left(r\frac{dT}{dr}\right)+k\frac{d^2T}{dz^2}+\Phi=\rho c_p V_r\frac{dT}{dr}-V_r\frac{dp}{dr} \qquad \ldots(3.5)$$

where,

$$\Phi=2\mu\left[\left(\frac{\partial V_r}{\partial r}\right)^2+\left(\frac{1}{r}\frac{\partial V_\theta}{\partial\theta}+\frac{V_r}{r}\right)^2+\left(\frac{\partial V_z}{\partial z}\right)^2+\frac{1}{2}\left(\frac{\partial V_\theta}{\partial r}-\frac{V_\theta}{r}+\frac{1}{r}\frac{\partial V_r}{\partial\theta}\right)^2+\frac{1}{2}\left(\frac{1}{r}\frac{\partial V_z}{\partial\theta}+\frac{\partial V_\theta}{\partial z}\right)^2+\frac{1}{2}\left(\frac{\partial V_r}{\partial z}+\frac{\partial V_z}{\partial r}\right)^2-\frac{1}{3}\left(\nabla\bullet q\right)^2\right]$$

$$\nabla\bullet q=\frac{\partial V_r}{\partial r}+\frac{V_r}{r}+\frac{\partial Vz}{\partial z}$$

Equation of state:

$$p=\rho R T \qquad \ldots(3.6)$$

In this formulation, the effects of turbulence are crudely included via the effective viscosity inclusion, whereby the laminar viscosity υ_l (or μ_l) is increased by an eddy constant viscosity υ_e (or μ_e) component.

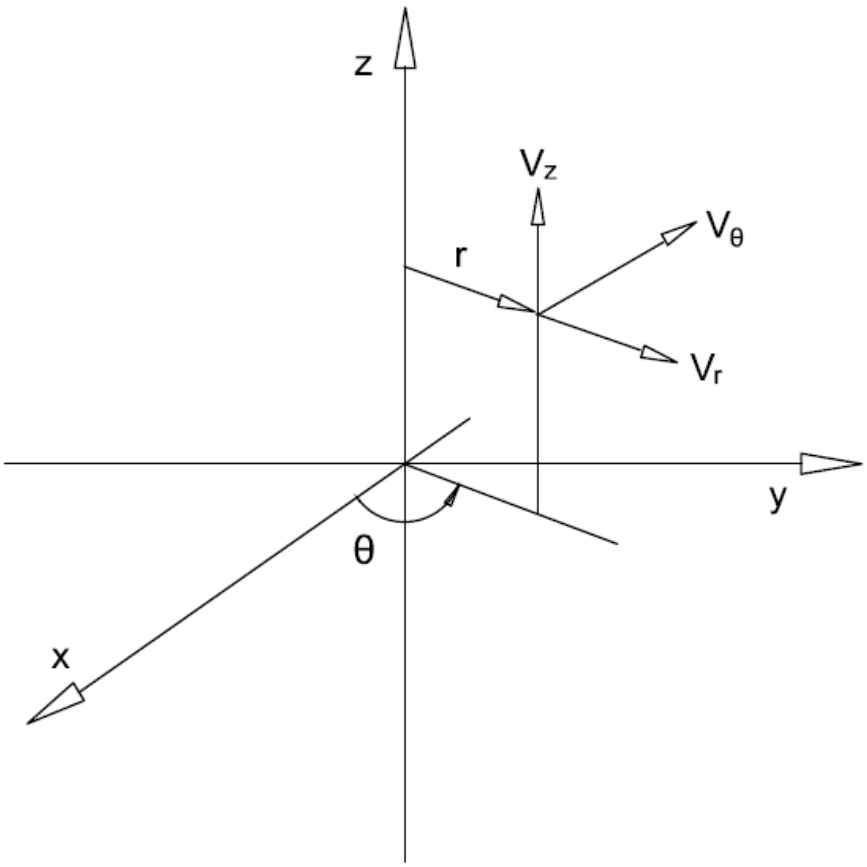

Figure 3.1. The coordinate system.

All the variables are defined in the nomenclature section, while the coordinate system is given in Fig. 3.1.

3.2. Simplification of the mathematical problem

The above system along with the required boundary conditions is difficult to solve. Thus, previous equations, however, could be reduced considering some simplifying assumptions.

The velocity field applicable to all classical vortices is taken as (Vatistas, 2006a):

$$q\left[V_r(r),\ V_\theta(r),\quad V_z = \quad z.fn(r)\ \right]$$

or in dimensionless form

$$q\left[u(\xi), V(\xi), h\, f(\xi)\right] \qquad \ldots(3.7)$$

Under the assumption given by Eq. (3.7), the dimensionless governing equations (Eqs. (3.1) – (3.6)) transform into:

Conservation of mass:

$$\frac{1}{\xi}\frac{\partial}{\partial\xi}\left(\beta u\xi\right) + \beta h = 0 \qquad \ldots(3.8)$$

$$1\delta \quad 1\delta$$

Radial momentum:

$$\mathrm{Re}\,\beta\left(u\frac{\partial u}{\partial\xi} + h\frac{\partial u}{\partial\zeta} - \frac{V^2}{\xi}\right) = -\mathrm{Re}\frac{\partial\Pi}{\partial\xi} + \frac{\partial}{\partial\xi}\left(\frac{1}{\xi}\frac{\partial u\xi}{\partial\xi}\right) + \frac{\partial^2 u}{\partial\zeta^2} \qquad \ldots(3.9)$$

$$\frac{1}{\delta}\ 1\quad \delta\ \ \delta\quad \delta\ \ \delta\quad 1 \qquad\qquad \frac{1}{\delta} \qquad\qquad \delta \qquad \delta$$

Tangential momentum:

$$\mathrm{Re}\frac{\beta u}{\xi}\left(\frac{\partial\left(V\xi\right)}{\partial\xi}\right) = \frac{\partial}{\partial\xi}\left(\frac{1}{\xi}\frac{\partial\left(V\xi\right)}{\partial\xi}\right) \qquad \ldots(3.10)$$

$$\frac{1}{\delta}\ 1\ \ \delta\quad 1 \qquad\qquad 1$$

Axial momentum:

$$\mathrm{Re}\,\beta\left(u\frac{\partial h}{\partial \xi}+h^2\right)=-\frac{\mathrm{Re}}{\zeta}\frac{\partial \Pi}{\partial \zeta}+\frac{1}{\xi}\frac{\partial}{\partial \xi}\left(\xi\frac{\partial h}{\partial \xi}\right) \qquad \ldots(3.11)$$

$$\frac{1}{\delta}\ \ 1\quad \delta\ \ \delta\quad \delta^2\qquad \frac{1}{\delta}\qquad\qquad \delta$$

Energy:

$$\frac{1}{\xi}\frac{\partial}{\partial \xi}\left(\xi\frac{\partial \Theta}{\partial \xi}\right)+\frac{\partial^2 \Theta}{\partial \zeta^2}+\mathrm{Pr}\left(\gamma-1\right)M_0^2 f=$$

$$1\qquad 1\qquad 1\ \ 1\qquad 1\ \ 1$$

$$\beta\,\mathrm{PrRe}\left(u\frac{\partial \Theta}{\partial \xi}+w\frac{\partial \Theta}{\partial \zeta}\right)-\mathrm{PrRe}\left(\gamma-1\right)M_0^2\left(u\frac{\partial \Pi}{\partial \xi}+w\frac{\partial \Pi}{\partial \zeta}\right) \qquad \ldots(3.12)$$

$$1\ \ 1\quad \frac{1}{\delta}\ \ \delta\ \ 1\quad \delta\ \ 1\qquad 1\quad \frac{1}{\delta}\qquad 1\ \ 1\qquad \delta\qquad \delta$$

where

$$f = 2\left(\left[\frac{\partial u}{\partial \xi}\right]^2 + \left[\frac{u}{\xi}\right]^2 + h^2 + \frac{1}{2}\left[\frac{\partial V}{\partial \xi} - \frac{V}{\xi^2}\right]^2 + \frac{1}{2}\left[\frac{\partial u}{\partial \zeta} + \zeta\frac{\partial h}{\partial \xi}\right]^2\right.$$

δ^2 δ^2 δ^2 δ^2 δ^2 δ^2 δ^2

$$\left. -\frac{1}{3}\left[\frac{\partial u}{\partial \xi} + \frac{u}{\xi} + h\right]^2 + \frac{1}{3}\left[\frac{1}{\xi}\frac{\partial(\beta u \xi)}{\partial \xi} + \beta h\right]^2 \right)$$

δ^2 δ^2 δ^2 δ^2 δ^2

Equation of state:

$$\Pi = \frac{\beta\Theta}{\gamma M_0^2} \qquad \text{…(3.13)}$$

1 1

Because we are considering strong (or intense) vortices, the basic assumption that u and h <<V is implemented. In terms of order of magnitude, if V is of order O(1), then u and h are of order O(δ) where δ = 1/Re. Typical value of delta (δ) for different vortices are provided below.

Table 3.1 Typical values of Reynolds numbers in a variety of vortices.

Type of vortex	$\mathbf{r_c}$ **(m)**	$\mathbf{V_{\theta(max)}}$ **(m/s)**	**Re**	**δ**
Tornadoes	10.0	60.0	4.0×10^7	10^{-7}
Dust devils	3.0	10.0	5.0×10^6	10^{-6}
Whirlpools	15.0	5.0	7.5×10^7	10^{-7}
Cyclone Chambers	0.2	0.5	6.7×10^5	10^{-5}
Bath tub vortices	0.2	0.1	2.0×10^4	10^{-4}
Aerodynamic vortices	1.0	10.0	6.7×10^5	10^{-5}

One can, thus, see that for most of the vortex flows; the typical value of δ is around 10^{-5}. Neglecting terms of order of O(δ) or smaller, reduces the above equations into considerably simpler form. It is worth noting that this basic assumption is the same as the one that had produced all the classical vortex models. As all the terms in Eqs. (3.8) and (3.10) are of the same order of magnitude, they will remain as they are. The rest will assume the simpler forms that are given underneath.

Radial momentum:

$$\frac{\beta V^2}{\xi} = \frac{\partial \Pi}{\partial \xi} \qquad \ldots(3.14)$$

The axial momentum Eq. (3.11) suggests that static pressure should not vary appreciably in the ζ- direction.

$$\mathrm{Re}\frac{\partial \Pi}{\partial \zeta} \approx \delta \qquad \text{or} \qquad \frac{\partial \Pi}{\partial \zeta} \approx \delta^2 \qquad \rightarrow \frac{\partial \Pi}{\partial \zeta} \cong 0 \qquad \ldots(3.15)$$

Therefore, it points out that the pressure should be sole function of ξ. In addition, from the ξ-momentum equation, the density must also depend on ξ alone and from the equation of state; the temperature must also depend on ξ alone.

Energy:

$$\frac{1}{\xi}\frac{d}{d\xi}\left(\xi\frac{d\Theta}{d\xi}\right)+\Pr\left(\gamma-1\right)M_0^2 f=\beta\,\mathrm{PrRe}\,u\frac{d\Theta}{d\xi}-\mathrm{PrRe}\left(\gamma-1\right)M_0^2 u\frac{d\Pi}{d\xi} \qquad \ldots(3.16)$$

where $f=\xi^2\left(\frac{d}{d\xi}\left[\frac{V}{\xi}\right]\right)^2$

These equations can be further simplified by letting $U=\beta\,\mathrm{Re}\,u$ & $H=\beta\,\mathrm{Re}\,h$ and replacing pressure gradient by its equivalent $\frac{\beta V^2}{\xi}$. The governing equations becomes:

Conservation of mass:

$$\frac{1}{\xi}\frac{d\left(U\xi\right)}{d\xi}+H=0 \qquad \ldots(3.17)$$

Radial momentum:

$$\frac{\beta V^2}{\xi}=\frac{d\Pi}{d\xi} \qquad \ldots(3.18)$$

Tangential momentum:

$$\frac{U}{\xi}\frac{d(V\xi)}{d\xi}=\frac{d}{d\xi}\left(\frac{1}{\xi}\frac{d(V\xi)}{d\xi}\right) \qquad \ldots(3.19)$$

Energy:

$$\frac{1}{\xi}\frac{d}{d\xi}\left(\xi\frac{d\Theta}{d\xi}\right)+\Pr U\frac{d\Theta}{d\xi}=-\Pr(\gamma-1)M_0^2\left(\frac{UV^2}{\xi}+\xi^2\left(\frac{d}{d\xi}\left[\frac{V}{\xi}\right]\right)^2\right)$$

…(3.20)

Equation of state:

$$\Pi=\frac{\beta\Theta}{\gamma M_0^2} \qquad \ldots(3.21)$$

3.3. Boundary conditions

In addition to the field equations, one requires the appropriate boundary conditions in order to solve the problem.

The necessary boundary conditions are, thus:

(i) At ξ=0,

$V(\xi)=U(\xi)=0$

and $\frac{dH(\xi)}{d\xi}=\frac{d\Theta(\xi)}{d\xi}=0$

(ii) At $\xi\to\infty$

$V(\xi)\xi\to 1$

$\Theta(\xi)\to 1$

$\gamma M_0^2\Pi(\xi)\to 1$ and $\beta(\xi)\to 1$

Chapter 4. Numerical Solution

In this thesis, Vatistas' (2006b) vortex model is used to simulate turbulent compressible vortices:

$$V = \xi\left(\frac{a+1}{a+\xi^4}\right)^m \qquad \ldots(4.1)$$

where a=0.7

Inserting Eq. (4.1) into the tangential momentum Eq. (3.19), the radial velocity (U) is determined.

$$U = m\left(\frac{\frac{8(m+1)\xi^7}{a+\xi^4} - 12\xi^3}{a+\xi^4-2\xi^4 m}\right) \qquad \ldots(4.2)$$

Integrating the energy Eq. (3.20) twice along with the boundary conditions yields the temperature.

$$\Theta(\xi) = -\int_0^{\xi} \frac{\int_0^x X.f_2(X)IF\,dX}{x.IF}dx + \int_0^{\infty} \frac{\int_0^x X.f_2(X)IF\,dX}{x.IF}dx + 1 \qquad \ldots(4.3)$$

Where X and x are dummy variables and

$$f_2(\xi) = \Pr(\gamma - 1)(a+1)^{2m} M_0^2 \frac{\xi^4}{\left(a+\xi^4\right)^{2m}} \left(\frac{16m^2\xi^2}{\left(a+\xi^4\right)^2} + m \frac{\frac{8(m+1)\xi^2}{a+\xi^4} - 12}{a+\xi^4 - 2\xi^4 m} \right) \quad \ldots(4.4)$$

$$IF = \exp\left(-\int_0^{\xi} f_1(x)\, dx \right) \quad \ldots(4.5)$$

$$f_1(\xi) = \left(\frac{\frac{8(m+1)\xi^7}{a+\xi^4} - 12\xi^3}{a+\xi^4 - 2\xi^4 m} \right) m \Pr \quad \ldots(4.6)$$

Differentiating the equation of state Eq. (3.21) w.r.t. ξ, it becomes

$$\frac{d\Pi}{d\xi} = \frac{1}{\gamma M_0^2} \left(\Theta \frac{d\beta}{d\xi} + \beta \frac{d\Theta}{d\xi} \right) \quad \ldots(4.7)$$

Using relation of radial momentum (ξ-momentum) Eq. (3.18), Eq. (4.7) becomes

$$\frac{d}{d\xi}\left(\ln(\beta\Theta) \right) = \gamma M_0^2 \frac{V^2}{\xi\Theta} \quad \ldots(4.8)$$

Integration of the above Eq. (4.8) and application of boundary condition for density when $\xi \to \infty$, gives:

$$\beta = \frac{c_1}{\Theta} \exp\left(\gamma M_0^2 \int_0^{\xi} \frac{V^2}{\xi\Theta} d\xi \right) \quad \ldots(4.9)$$

where

$$c_1 = \frac{1}{\exp\left(\gamma M_0^2 \lim_{L \to \infty} \int_0^{L} \frac{V^2}{\xi\Theta} d\xi \right)} \quad \ldots(4.10)$$

The pressure can then be calculated from the equation of state Eq. (3.21) or from Eq. (4.7). The equation for temperature (Eq. (4.3)), density (Eq. (4.9)) and pressure (Eq. (4.7)) are solved using 1/3 composite Simpson's rule with the combination of in-built 'quadl' function within error of 10^{-6} on the mathematical platform 'MATLAB' for Prandtl number, Pr = 2/3 and different Mach numbers 0.4, 0.6 and 0.8. The results from numerical integration are compared with the results obtained using finite difference method in the work of Badwal (2014).

All the calculations done in this thesis are done for Pr = 2/3. The reason behind using this particular value of Prandtl number is that it gives an exact solution for energy equation for a laminar vortex (Vatistas, 2006a). The Prandtl number for most of gases lies between 0.680 for helium to 0.716 for nitrogen. Even if, one uses Prandtl numbers within the previous interval, it will produce a deviation in temperature of no more than 0.5% (Badwal, 2014).

It can be noted that the integration limits of temperature (Θ) in the Eq. (4.3) and density (β) in the Eq. (4.10) include infinite limits. The following question then arises: how far infinity will be? It can be answered with the help of numerical calculations. The relative difference between value of temperature at center i.e. $\Theta_{(\xi=0)}$ is calculated at various values of infinity i.e. ξ_∞ and is found to be 7.2×10^{-4} when ξ_∞=200 and ξ_∞=400 (Badwal, 2014). Therefore, in order to economize on the computations, a radius of 200 i.e. ξ_∞=200 is found to be adequate (Badwal, 2014).

The optics formulation will consider the gas density varying only in y-direction (Fig. 4.1) as explained by Goldstein (1996). The intensity on the image plane, E, will be:

$$E = \frac{1}{\lim_{\delta y \to 0} \frac{\delta y_{impl}}{\delta y}} E_{\infty} \qquad \ldots(4.11)$$

where $\delta y_{impl} = \delta y + l\delta\alpha$

or $$\Sigma = \frac{E}{E_{\infty}} = \frac{1}{\left|1 + l\frac{\partial \alpha}{\partial y}\right|} \qquad \ldots(4.12)$$

There could be situations that the light rays under consideration, when refracted, can cross over. Therefore, in order to make sure that Σ always remain positive, the absolute sign has been incorporated.

The angle α is given by (Bagai & Leishman, 1993)

$$\alpha = \frac{1}{\eta_{\infty}} \int_{l_1}^{l_2} \frac{\partial \eta}{\partial y} dz = \frac{l_2 - l_1}{\eta_{\infty}} \frac{d\eta}{dy} \qquad \ldots(4.13)$$

Therefore,

$$\Sigma = \frac{1}{\left|1 + \frac{l(l_2 - l_1)}{\eta_{\infty}} \frac{\partial^2 \eta}{\partial y^2}\right|} \qquad \ldots(4.14)$$

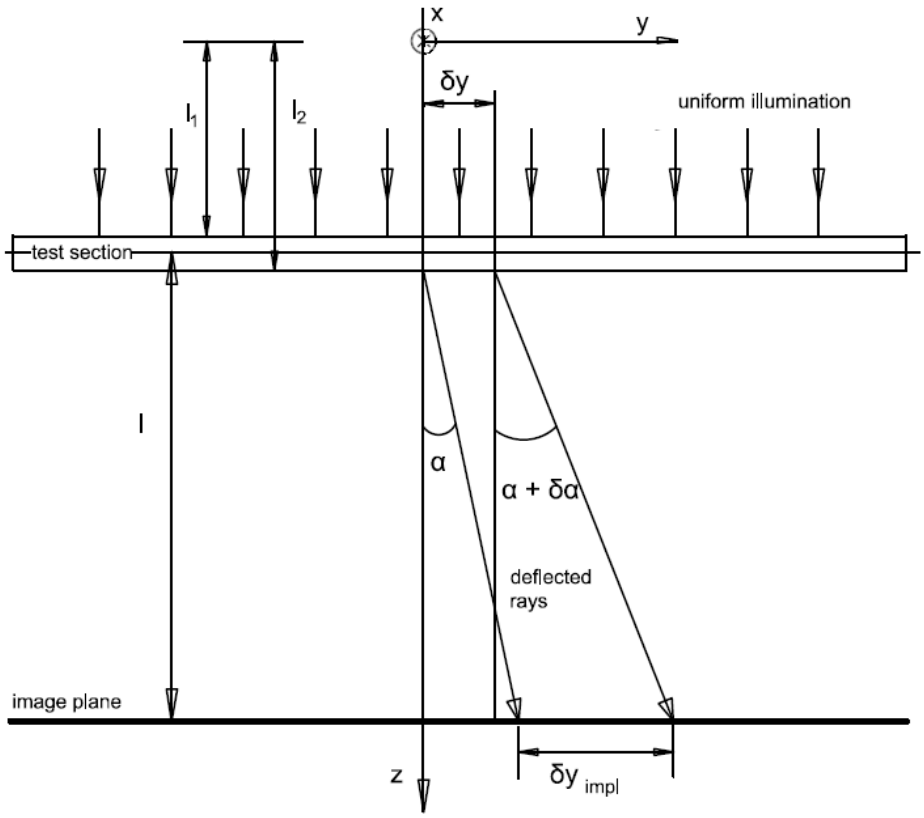

Figure 4.1. The arrangement for the optical side of the problem (Adaption from Vatistas, 2006c).

The refractive index is the ratio of speed of light in vacuum to speed of light in the medium under consideration. As the speed of light in dilute gases is moderately less than that in vacuum (Liepmann & Roshko, 1957), one could use the Gladstone-Dale relation to model the event without loss of physics.

$$\left(\frac{\eta-1}{\rho}\right)=C \qquad \ldots(4.15)$$

$$\Sigma=\frac{1}{\left|1+\frac{l\left(l_1-l_2\right)C}{\eta_\infty}\frac{\partial^2\rho}{\partial y^2}\right|} \qquad \ldots(4.16)$$

The above expression in polar geometry, assuming axisymmetric density variation, is:

$$\Sigma = \frac{1}{\left|1 + \frac{l(l_1 - l_2)C}{\eta_\infty}\left(\frac{1}{r}\frac{\partial \rho}{\partial r} + \frac{\partial^2 \rho}{\partial r^2}\right)\right|} \qquad \ldots(4.17)$$

or in dimensionless form

$$\Sigma = \frac{1}{|1 + \Lambda\Delta|} \qquad \ldots(4.18)$$

where

$$\Lambda = \frac{\lambda(\lambda_2 - \lambda_1)\sigma}{\eta_\infty}$$

$$\Delta = \frac{1}{\xi}\frac{\partial \beta}{\partial \xi} + \frac{\partial^2 \beta}{\partial \xi^2}$$

$$\lambda = \frac{l}{r_c} \quad , \quad \lambda_1 = \frac{l_1}{r_c} \quad , \quad \lambda_2 = \frac{l_2}{r_c} \qquad and \quad \frac{\sigma}{\sigma_\infty} = C$$

The expression for the intensity (Σ) is solved using a central difference of finite scheme with step size as 0.001 and number of steps equal to 200,000 for Λ values of 5 and 25. The various profiles of the intensity (Σ) will be presented in the next chapter.

Chapter 5. Results and discussion

In the previous chapter, the numerical method used to solve the mathematical equations was outlined. The results obtained are presented and discussed in this chapter.

One of the most basic of the thermodynamic properties that is required to solve the present problem is the temperature (Θ). The last was determined solving numerically the energy equation that provided Eq. (4.3). The density (β) is then calculated from Eq. (4.9). The results of the temperature (Θ) radial distributions for vortex Mach numbers equal to 0.4, 0.6 and 0.8 are plotted in Fig. 5.1.

It is evident from Fig. 5.1 that as the fluid travels from far towards the vortex center; its temperature first increases until the radius (ξ) of 4.06 and then reduces until it reaches the lowest temperature at the vortex center. The higher the Mach number is, the higher is the maximum temperature and lower is the minimum temperature at the vortex center.

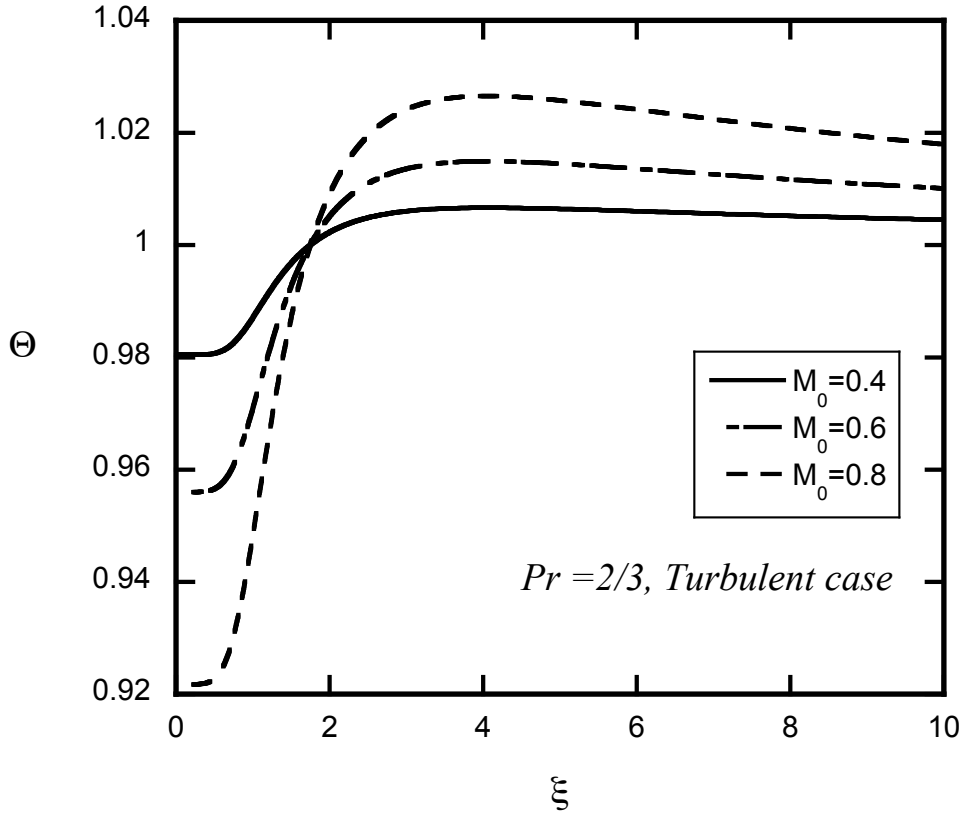

Figure 5.1 Radial distribution of temperature (Θ) for different Mach numbers.

This behavior of temperature (Θ) can be explained with the help of radial rate of change temperature equation (Badwal, 2014), which is given below:

$$-\frac{d\Theta}{d\xi} = \Pr(\gamma-1)M_0^2 \frac{\int_0^{\xi} f\xi\lambda\, d\xi}{\xi\lambda} + \Pr(\gamma-1)M_0^2 \frac{\int_0^{\xi} UV^2\lambda\, d\xi}{\xi\lambda} \qquad \ldots(5.1)$$

$$\begin{pmatrix} Heating.of.fluid \\ element.due.to. \\ friction \end{pmatrix} \qquad \begin{pmatrix} Cooling.of.fluid.element. \\ due.to.\exp ansion \end{pmatrix}$$

The negative sign in front of the radial derivative of temperature designates a converging flow i.e. the fluid is moving from the outer periphery towards the axis of the vortex. As fluid elements move along the flow direction, they come under the influence of two elementary effects: heating due to viscous forces that tends to increase their temperature and cooling due to their dilation. This is illustrated in Fig. 5.5 of Badwal's (2014) thesis that at the outer periphery the contribution of friction is higher than cooling and thus, the fluid elements get hotter while near the vortex center the overpowering effects of cooling over friction makes the temperature to drop.

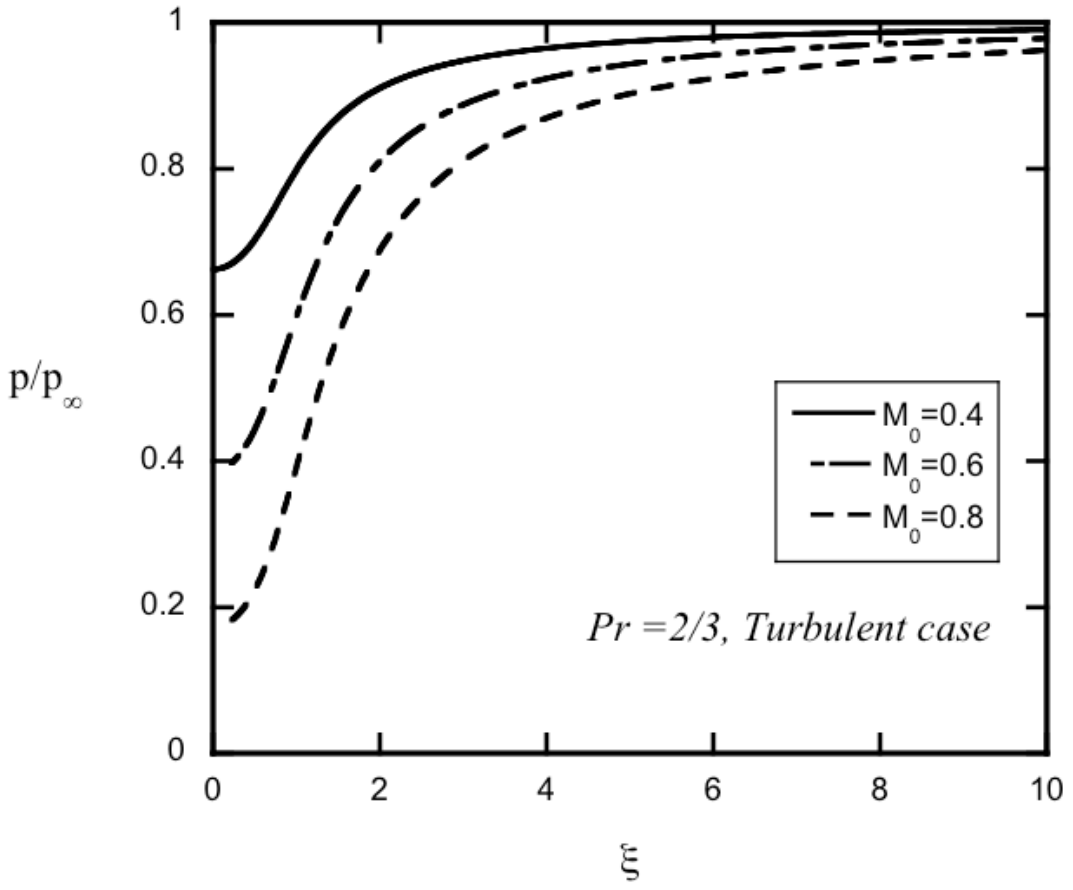

Figure 5.2. The plot of dimensionless pressure (Π) along the radial direction for different Mach numbers.

The radial distribution of pressure (Π) is plotted in Fig. 5.2 where it can be seen that it decreases monotonically along the flow direction. There is progressive change in pressure values from about thrice the vortex core radius. There is a steep change in pressure near and inside the core.

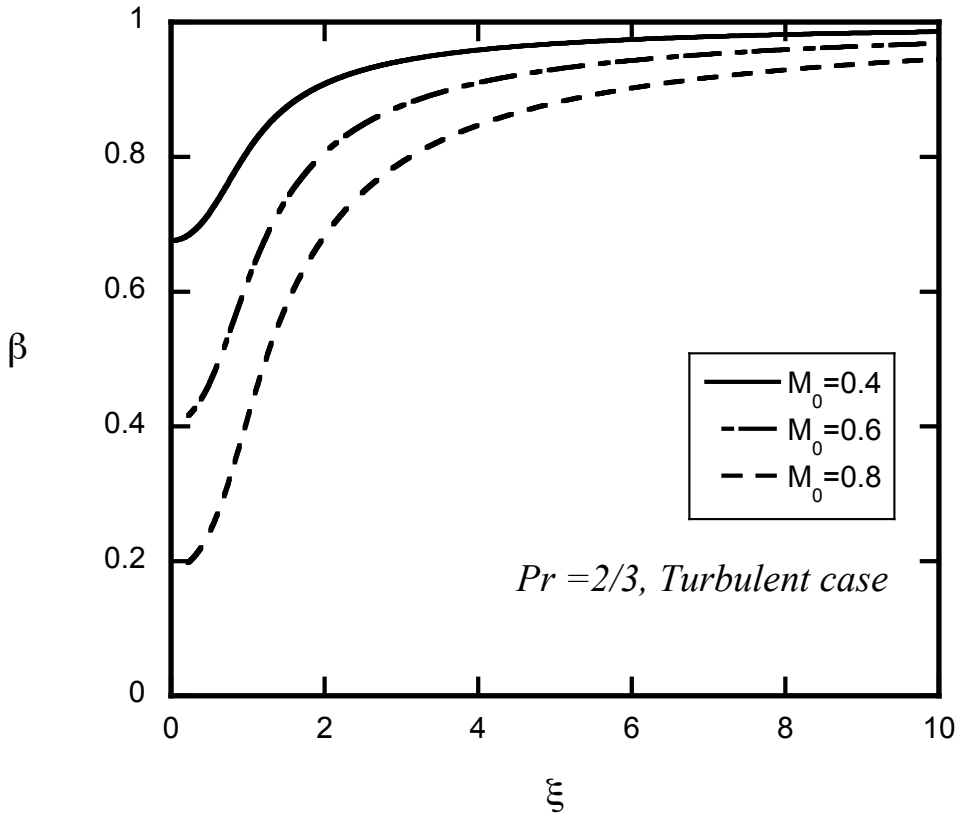

Figure 5.3. Radial distribution of density (β) for different Mach numbers.

This behavior of pressure profile along radial direction can be explained along with density profile as follows. For most of the radial interval $0 \leq \xi < \infty$, the tangential velocity for a turbulent vortex is larger than the laminar (especially in the outer periphery). The last will generate a stronger centrifugal acceleration,

$$\alpha_\xi = \frac{V^2}{\xi} \qquad \ldots(5.2)$$

for a turbulent than for a laminar vortex (see Fig. 5.4).

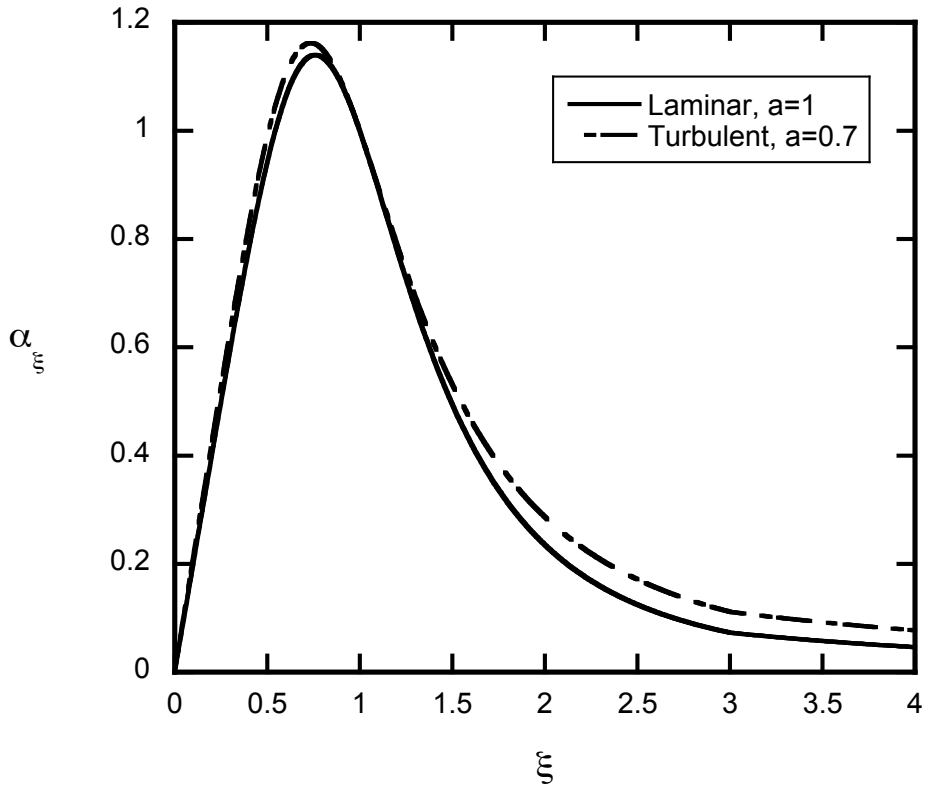

Figure 5.4. Comparison of radial distribution of Centrifugal acceleration of turbulent and laminar vortices.

The combined effect of the centrifugal force per unit volume is given by,

$$F_\xi = \beta \frac{V^2}{\xi} \qquad \ldots(5.3)$$

From the radial momentum equation, we have that the variation of the pressure must balance the centrifugal force.

$$\frac{d\Pi}{d\xi} = \beta\, \alpha_{\xi} \qquad \ldots(5.4)$$

Therefore, the pressure in a turbulent vortex starting at the same value (far field) as the laminar vortex, should decreases along the flow direction more rapidly until $\xi = 1.9$ and then, decrease at a slower pace. However, the cumulative prior drop will carry on to the end, thus, produce a larger pressure deficit at the center. Consequently, at the center of the turbulent vortex the gas will also be thinner (lower density).

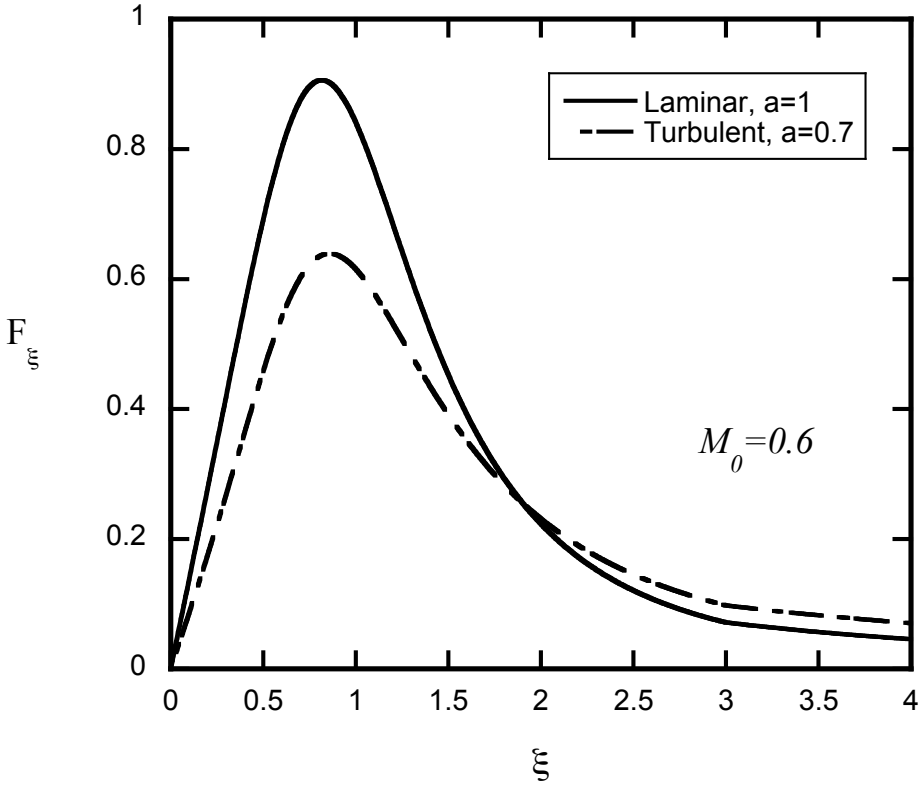

Figure 5.5. Comparison of radial distribution of centrifugal force per unit volume of turbulent and laminar vortices.

Every mathematical representation of real events must in addition to the conservation equations should also obey the entropy increase axiom (second law of thermodynamics). It has been proved recently by Badwal (2014) that this turbulent compressible vortex formulation used in this thesis, does indeed respects the second law of thermodynamics.

The major results of this thesis i.e. the optics results will now be presented in terms of the light intensity profile. The brightness of the shadows casted on the image plane depends on the curvature of the density profile or correspondingly (by analogy) on the shape of the free liquid

surface (pressure surface). The distribution of intensity (or luminosity) Σ along the radial direction is shown in Fig. 5.6 for different Mach numbers and Λ=5.

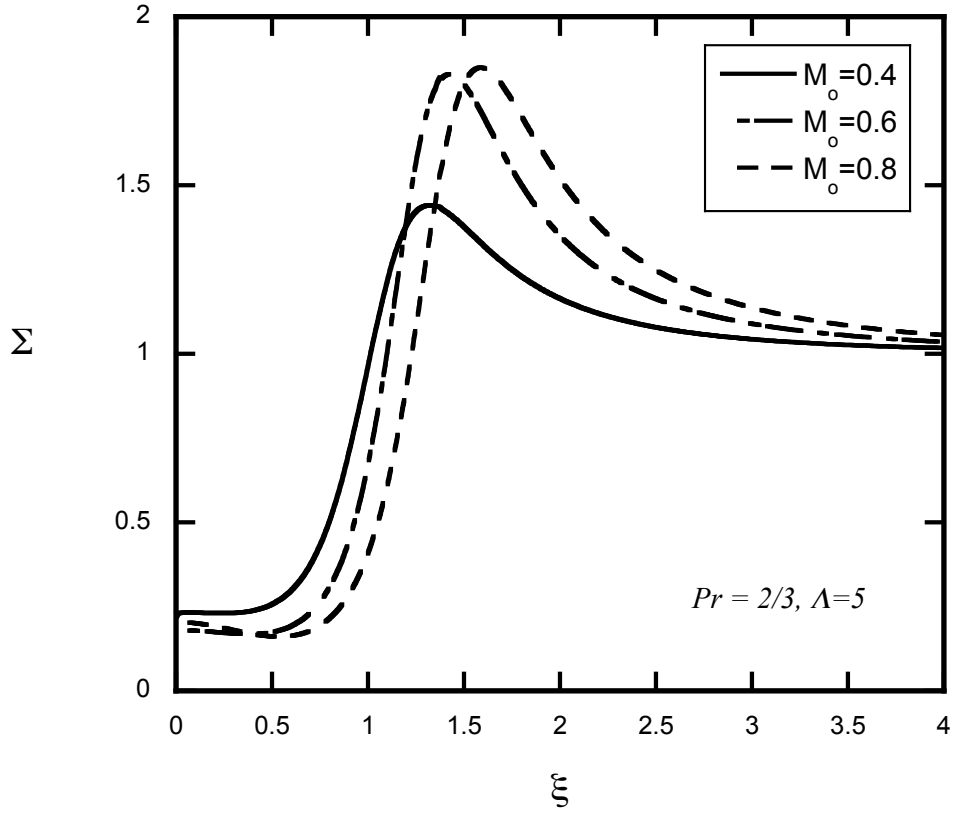

Figure 5.6. The radial distribution of Intensity for focal length of 5 for different Mach numbers.

As illustrated in Fig. 5.6, the light intensity values near the vortex core (ξ = 1) are generally less than the background values. The last indicates that a dark disk should appear on the image plane. At a radius slightly larger than the core, where the luminosity achieves a positive maximum, will give rise into a bright ring (or halo). At larger radii, the intensity will approach asymptotically to the background value of one. This behavior is evident in the observed shadowgraph of Bagai and Leishman (1993) shown in Fig. 2.6. Also, in the very recent paper of Bauknecht et al. (2014), the side view shadowgraphs obtained using the Background-Oriented

Schlieren Technique, identified a similar shadow structures in helicopter blade vortices (their Fig. 6 (c) and (d)).

Because the gas-dynamic and the liquid vortex (with an interface) phenomena are analogous, the two must produce similar shadows. The last is sufficiently clear in the observed shadowgraphs of the liquid vortices given in Figs. 2.5 (Sterling et al., 1987) and 1.4 (c) (Vatistas, 2011)), respectively.

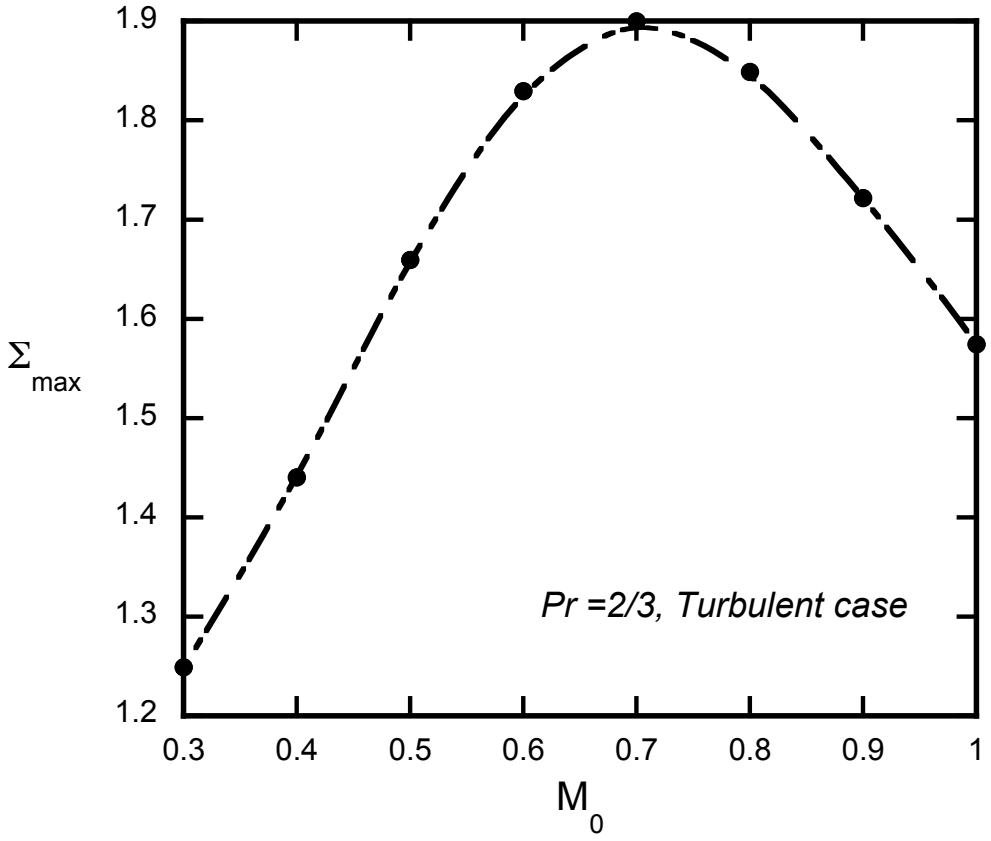

Figure 5.7. Variation of the maximum light intensity with the vortex Mach number.

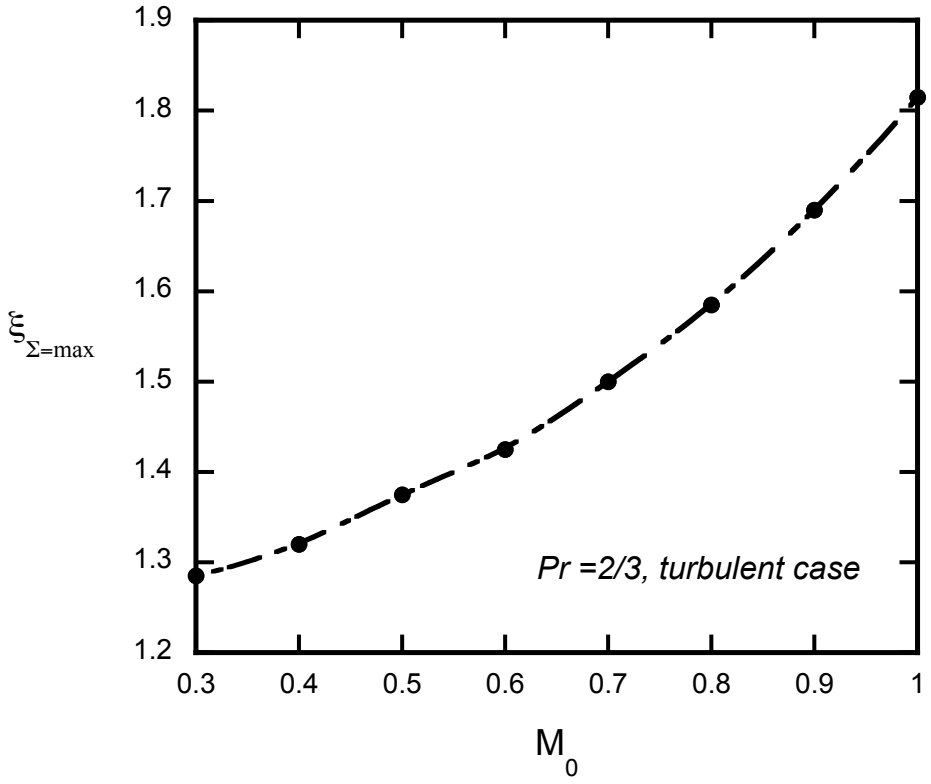

Figure 5.8. Variation of the radial distance of the maximum light intensity location with the vortex Mach number.

The degree of illumination depends on the vortex Mach number. A close examination of Fig. 5.7 shows that the maximum intensity values increases as the Mach number augments, it reaches a maximum at about 0.7, and then weakens afterwards. As the Mach number increases, its location is seen to move away from the vortex center (see Fig. 5.8).

The plot shown in the Fig. 5.6 also suggests that darkest area in the image plane is not at the vortex core but it is rather displaced outwards. But it always resides within the vortex core, which is also in agreement with observed shadowgraphs of Sterling et al. (1987) and Bagai and Leishman (1993).

Depending on the value of the focal length Λ, the shadows casted on the image plane can be dramatically different. Two focal lengths i.e. $\Lambda = 5$ and $\Lambda=25$ were tested and the results for $M_0 = 0.4$, 0.6 and 0.8 are shown in Figs. 5.9-5.11. It is interesting to note that although the values of intensity and location of the caustic(s) may be different, their qualitative appearance for turbulent vortices are alike to their laminar counterpart.

For low Λ, the light intensity profile begins with a dark disk at the center of the vortex characterized by low values of Σ. As the radius increases, Σ augments reaching a maximum where the caustic exists and then, drops asymptotically to the background illumination values. Typical computed shadowgraph is shown in the Fig. 5.12 (a).

Focusing at larger depth (high Λ values), two caustics may appear. Beginning once more, with a dark disk at the center of the vortex, the light intensity increases with the radius reaching a first maximum, which designates the inner caustic. Past the first halo, the value of Σ drops, followed by a second caustic. At larger radii, Σ drops asymptotically to the background illumination values but with values that are greater than that corresponding to low Λ. The area between the first and second caustic is dimmer than the two caustics and for larger M_0 values, its illumination Σ can be lower than the background value of one, thus, forming a dark circular ring. The inner caustic is always thinner than the outer (see Fig. 5.12 (b)). It is interesting to mention a propos that in the sunspot picture given in Fig. 1.2 (b), the diffused second halo in heliograph image of Hale (2006) is indeed thicker than the first.

Although the caustics appear as mathematical singularities, these are not. The maximum value at each caustic may indeed be very large; it is not, however, infinite. The transition from

one to two caustics is sudden (catastrophic). The last may suggest that there may exist bifurcating solutions for Σ.

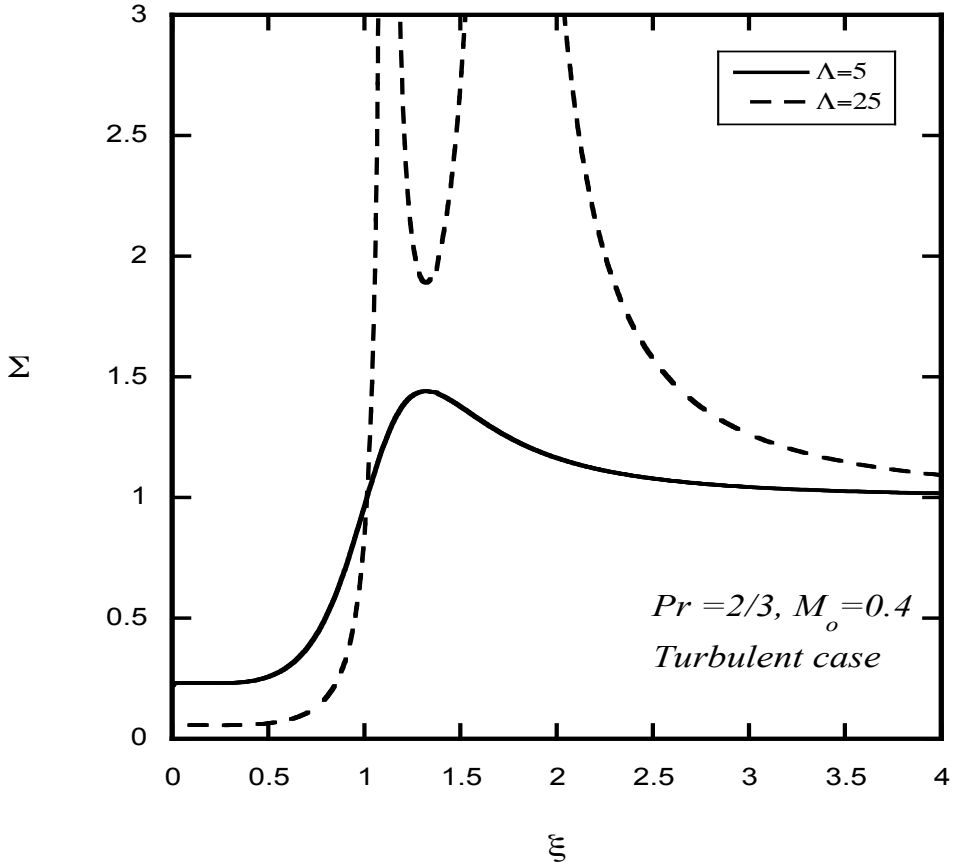

Figure 5.9. The intensity profiles for Λ=5 and Λ=25 in radial direction for Mach number, M_0 = 0.4. For the focal length of 25, two caustics with the first being narrower than the second, emerge.

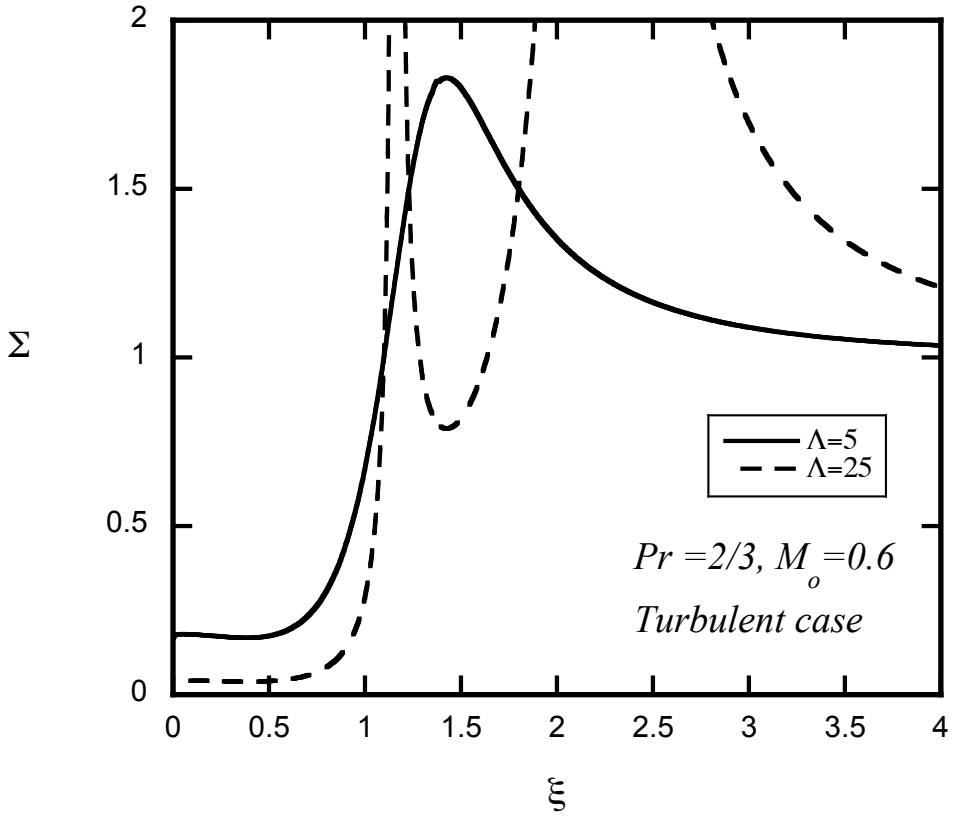

Figure 5.10. The intensity profiles for Λ=5 and Λ=25 in radial direction for Mach number, M_0 = 0.6.

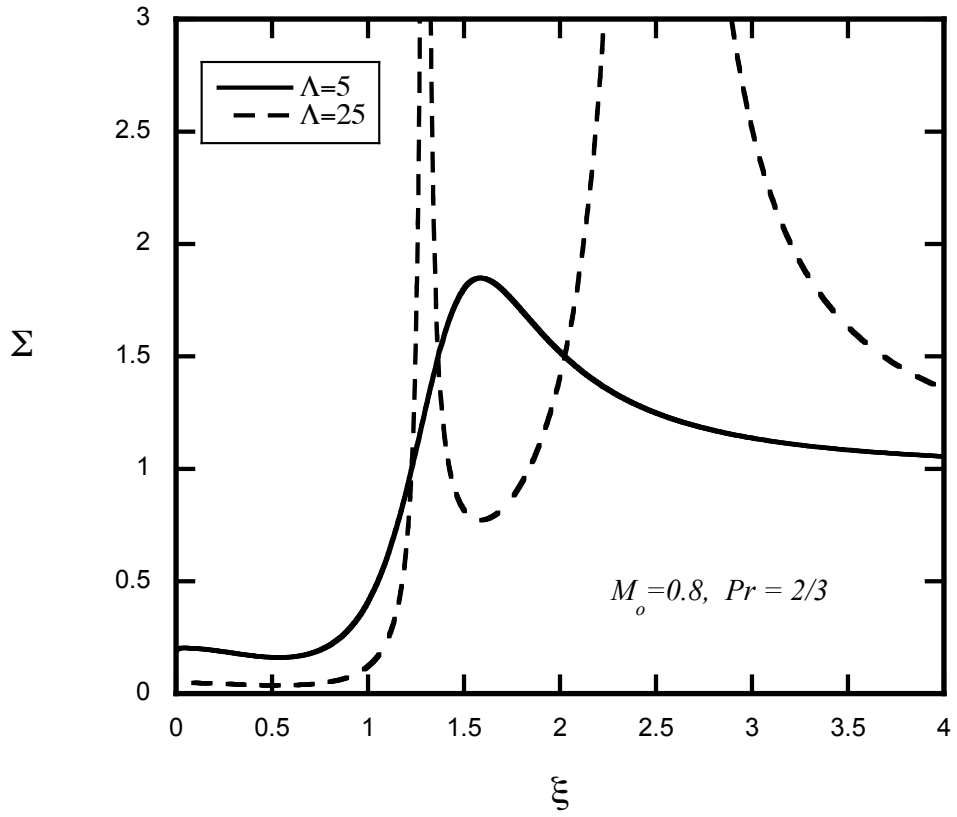

Figure 5.11. The intensity profiles for Λ=5 and Λ=25 in radial direction for Mach number, M_0 = 0.8.

Also alike to the vortices in the case of two caustics, it is also evident that the illumination of the dark disk becomes dimmer as the vortex Mach number increases.

Swanson and Light (1992) presented experimental shadowgraphs of a compressible vortex generated by a tilt rotor blade revealed a peculiar shadow signature that in addition to the standard dark disk halo arrangement, also included a strange set of a pair of alternating dark and bright circular bands. Parthasarthy et al. (1987) and Bagai and Leishman (1993) proposed that perhaps this unseen previously manifestation might be due to a very unusual air density profile, commenting also that the cause behind this unusual property remains to be discovered. As was

the case with the laminar compressible formulation, the present analysis shows that such light structure may also appear at larger l (or L) values in the turbulent case. The latter optical manifestation is also analogous to the two caustics shadowgraphs of liquid vortices visualized by Berry and Hajnal (see Fig. 2.4).

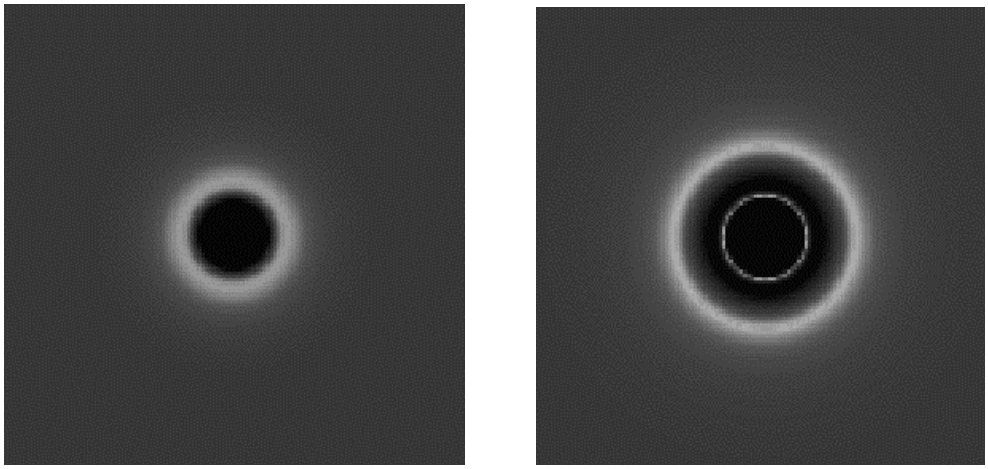

(a) (b)

Figure 5.12. Typical Computed vortex shadowgraphs (a) Λ=5 and (b) Λ=25 (Vatistas, 2006a).

As mentioned earlier in chapter 1, this thesis is an extension of Vatistas' work on optics of compressible laminar vortices into compressible turbulent vortices. Therefore, comparison has been made between optics of laminar and turbulent vortices.

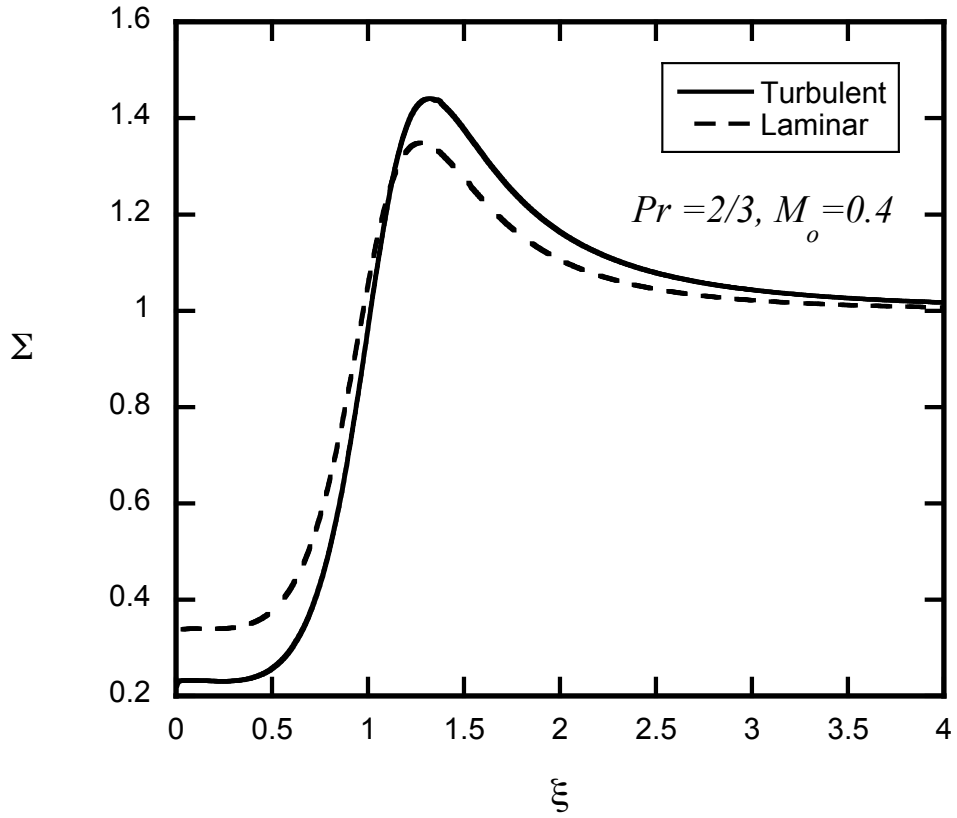

Figure 5.13. Plot of intensity (Σ) for laminar and turbulent case for Mach number 0.4 and Λ=5.

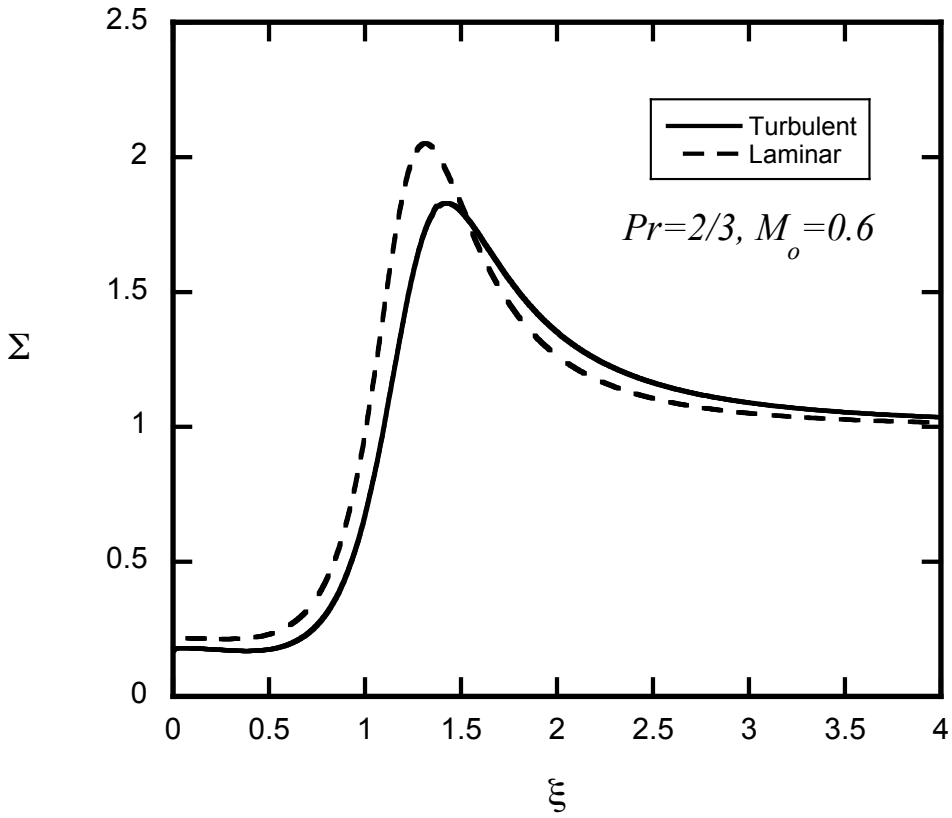

Figure 5.14. Plot of intensity (Σ) for laminar and turbulent case for Mach number 0.6 and Λ=5.

.

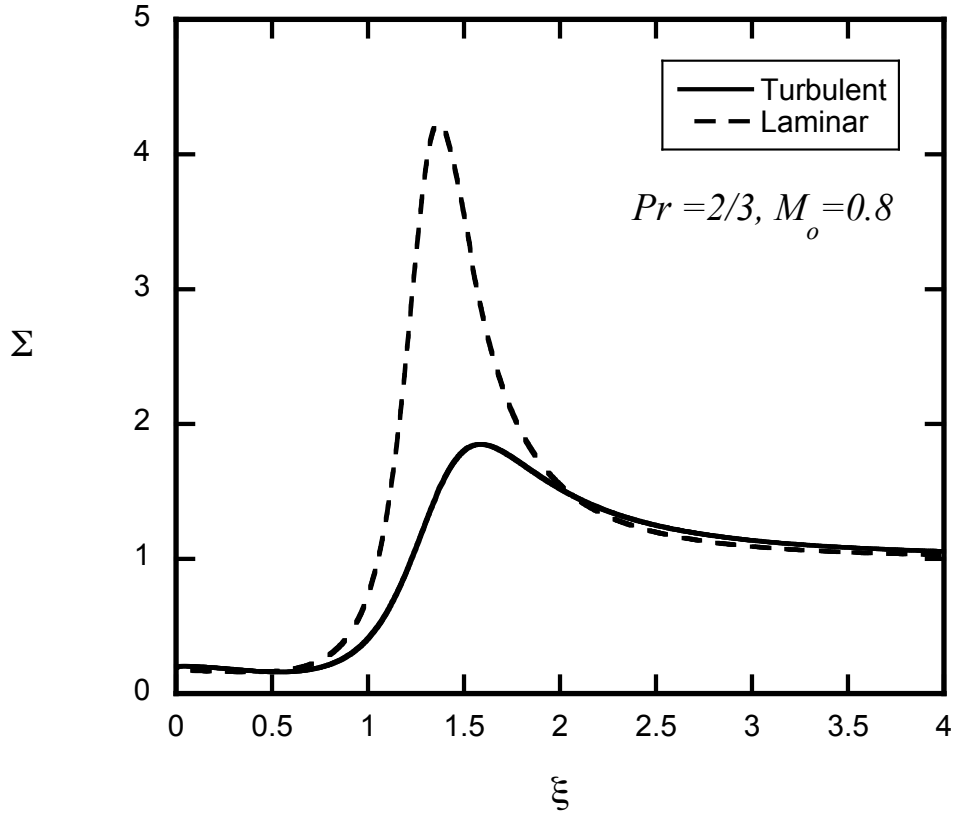

Figure 5.15. Plot of intensity (Σ) for laminar and turbulent case for Mach number 0.8 and Λ=5.

The results for intensity (Σ) are plotted in radial direction of fluid flow for laminar and turbulent case for specific Mach numbers i.e. M_0 = 0.4, 0.6 and 0.8 for Λ=5 are plotted in Figs. 5.13-5.15. It can be seen from this set of graphs that besides when M_0 = 0.4, the values of the maximum intensity (Σ) is higher for laminar than the turbulent vortex. In fact, for M_0 = 0.8, the laminar intensity Σ is about twice than the corresponding turbulent.

The location of the halo occurs further away from the vortex center in turbulent vortices. Also, in general, at the outer periphery turbulent vortices are brighter than the laminar.

Chapter 6. Conclusion

This thesis dealt for the first time with the refracted shadows produced by turbulent compressible vortices. The construction of the theory was accomplished by extending the previous laminar approach to include the effects of turbulence.

The pressure, temperature and density were obtained by solving numerically the conservation of mass, momentum and energy equations together with the equation of state for the case of a turbulent vortex evolving in a compressible, viscous, heat conducting and calorically perfect gas in a domain of infinite extend. The radial distribution of the light intensity was then, inferred via the past general mathematical relation that connects the density to light intensity of the shadowgraphs casted on an image plane by light ray refraction passing through the variable density gas.

The differences in luminosity of laminar and turbulent vortices with Mach numbers ranging from 0.4 to 0.8 were also compared. The darkness of the central disc and luminosity of the bright ring are found to be a function of the vortex Mach number: higher the Mach numbers produced darker central disks and dimmer halos. Vortices of the turbulent kind were found to produce different shadow signatures than the laminar. These differences amongst the two types of vortices were quantitative nature than qualitative. Alike to the laminar case and depending on the focal length, turbulent vortices could also generate the previously disputed two caustics. The last effect is shown to generate the combination of dark circular area near the vortex center,

followed by a thin halo, which is subsequently succeeded by a dim ring that is followed by a thicker corona.

Chapter 7. Future Work

In the present study, given a turbulent vortex generated in a compressible unconfined gas under a uniform illumination, the variation of light intensity was determined. The contribution can be used to explain several problems in science and technology. However, in order to increase its practical value, the inverse solution to the problem at hand could be attained, by answering the following question. How the fluid properties like pressure, temperature, density and the tangential velocity component could be recovered given an experimentally obtained shadowgraph? If one successfully answers the last question then the methodology can be used as a non-intrusive optical measuring tool for compressible vortices.

Several geophysical and aerodynamic vortices are of the two-celled type. Although, mathematical formulations for the incompressible kind exist, there is no contribution in the open literature for multi-celled compressible vortices. Consequently, their optics is also unknown. Using the present contribution, it will be very beneficial if one extends even the incompressible laminar one celled-vortices into multi-cell compressible vortices. Performing the last then their shadowgraphs can be easily theoretically obtained.

There is very little information on the experimental side of the problem. Any contribution towards extensive experimental validations of the present and past theoretical studies on optics will be highly desirable.

References

Aboelkassem, Y., & Vatistas, G. H. (2007). On the refracted patterns produced by liquid vortices. *Acta Mechanica Sinica, 23*(1), 11-15.

Badwal, G. S. (2014). A model for turbulent compressible vortices.

Bagai, A., & Leishman, J. G. (1993). Flow visualization of compressible vortex structures using density gradient techniques. *Experiments in Fluids, 15*(6), 431-442.

Bauknecht, A., Merz, C. B., Raffel, M., Landolt, A., & Meier, A. H. (2014). Blade-Tip Vortex Detection in Maneuvering Flight Using the Background-Oriented Schlieren Technique. *Journal of Aircraft*, 1-10.

Berry, M. V., & Hajnal, J. V. (1983). The shadows of floating objects and dissipating vortices. *Optica acta, 30*(1), 23-40. doi: 10.1080/713821046

Burgers, J. M. (1948). A mathematical model illustrating the theory of turbulence. *Adv. in Appl. Mech., 1*, 171-199.

Chigier, N., & Corsiglia, V. (1971). Tip vortices-velocity distributions. *Proceedings of the American Helicopter society, 27th Annual forum*.

Dosanjh, D., Gasparek, E., & Eskinazi, S. (1962). Decay of a viscous trailing vortex. *Aeronautical Quarterly, 13*(2), 167-188.

Goldstein, R. (1996). Fluid mechanics measurements: *CRC Press*.

Hale, G. E. (1924). Sun-spots as magnets and the periodic reversal of their polarity. *Nature, 113*, 105-112.

Hale, G. E. (2006). The New Heavens. *Project Gutenberg eBook*.

Helmholtz, H. v. (1858). Uber die Integrale der hydrodynamischen gleichungen, welche den wirbelbewegungen entsprechen. *Journal für die reine und angewandte Mathematik, 55*, 25-55.

Kiehn, R. M. (1987). Falaco solitons,- A topological defect in a swimming pool. *rmkarXiv: grqc/0101098*.

Landau, L., & Lifshitz, E. (1987). Fluid Mechanics, V. 6 of Course of Theoretical Physics, 2nd English edition. Revised: Pergamon Press, Oxford-New York-Beijing-Frankfurt-San Paulo-Sydney-Tokyo-Toronto.

Liepmann, H., & Roshko, A. (1957). Elements of Gasdynamics John Wiley & Sons. *New York*.

Light, J. S., Swanson, A. A., & Norman, T. R. (1992). Application of the Wide‐Field Shadowgraph Technique to Helicopters in Forward Flight. *Journal of the American Helicopter Society, 37*(2), 23-28.

Merzkirch, W. (1974). Flow visualization: *Elsevier*.

Norman, T. R., & Light, J. S. (1986). Rotor tip vortex geometry measurements using the wide-field shadowgraph technique *4th Applied Aerodynamics Conference*: American Institute of Aeronautics and Astronautics.

Parthasarathy, S., Cho, Y., & Back, L. (1987). Wide-field shadowgraphy of tip vortices from a helicopter rotor. *AIAA Journal, 25*(1), 64-70.

Porter, C. O. (2011). *The optical environment from the tip vortices of a helicopter in different flight regimes*: University of Notre Dame, Indiana.

Ramasamy, M., & Leishman, J. G. (2006). A generalized model for transitional blade tip vortices. *Journal of the American Helicopter Society, 51*(1), 92-103.

Rankine, W. J. (1858). A manual of applied mechanics: R. Griffin (London).

Saffman, P., & Baker, G. (1979). Vortex interactions. *Annual Review of Fluid Mechanics, 11*(1), 95-121.

Scully, M. (1975). Computation of helicopter rotor wake geometry and its influence on rotor harmonic airloads. *Massachusetts Institute of Technology.*

Sterling, M., Gorman, M., Widmann, P., Coffman, S., Strozier, J., & Kiehn, R. (1987). Why are these disks dark? The optics of Rankine vortices. *Physics of Fluids (1958-1988), 30*(11), 3624-3626.

Sullivan, R. D. (1959). A Two-Cell Vortex Solution of the Navier-Stokes Equations. *Journal of the Aerospace Sciences, 26*(11), 767-768. doi: 10.2514/8.8303

Swanson, A. A., & Light, J. S. (1992). Shadowgraph flow visualization of isolated tiltrotor and rotor/wing wakes. *Paper presented at the AHS, Annual Forum, 48 th, Washington, Proceedings.*

Thompson, P. A. (1972). Compressible Fluid Dynamics: McGraw-Hill, Sec.

Van Dyke, M. (1982). An album of fluid motion. *Parabolic Press, Stanford California*.

Vatistas, G. H. (1998). New Model for Intense Self-Similar Vortices. *Journal of Propulsion and Power, 14*(4), 462-469. doi: 10.2514/2.5323

Vatistas, G. H. (2006a). The optics of the compressible N= 2 vortex. *Transactions of the Canadian Society for Mechanical Engineering, 30*(1), 143-166.

Vatistas, G. H. (2006b). Simple Model for Turbulent Tip Vortices. *Journal of Aircraft, 43*(5), 1577-1579. doi: 10.2514/1.22477

Vatistas, G. H. (2011). Sunspots are in many ways similar to terrestrial vortices. *arXiv preprint arXiv:1110.1215*.

Vatistas, G. H., & Aboelkassem, Y. (2006a). Extension of the Incompressible n = 2 Vortex into Compressible. *AIAA Journal, 44*(8), 1912-1915. doi: 10.2514/1.18511

Vatistas, G. H., & Aboelkassem, Y. (2006b). Space-Time Analogy of Self-Similar Intense Vortices. *AIAA Journal, 44*(4), 912-917. doi: 10.2514/1.18200

Vatistas, G. H., Aboelkassem, Y., & Siddiqui, K. (2005). Time Decay of n Family of Vortices. *AIAA Journal, 43*(6), 1389-1391. doi: 10.2514/1.13238

Vatistas, G. H., & Ait Abderrahmane, H. (2008). Optical effects of wake liquid vortices. *Journal of visualization, 11*(2), 112-112.

Vatistas, G. H., & Badwal, G. S. (April 2014). A simple model for turbulent compressible vortices. *Journal of fluids engineering, Under review*.

Vatistas, G. H., & Badwal, G. S. (March, 2014). The thermal similarity amongst tornadoes and vortex-tubes. *Journal of Meteorology and Atmospheric Physics, Under Review*.

Vatistas, G. H., Kozel, V., & Mih, W. (1991). A simpler model for concentrated vortices. *Experiments in Fluids, 11*(1), 73-76.

Vatistas, G. H., Lin, S., & Kwok, C. (1986). Theoretical and experimental studies on vortex chamber flows. *AIAA Journal, 24*(4), 635-642.

Appendix A

Solution of the energy equation

The energy equation is given as

$$\frac{1}{\xi}\left(\frac{d}{d\xi}\left(\xi\frac{d\Theta}{d\xi}\right)\right)-\Pr U\frac{d\Theta}{d\xi}=-\Pr(\gamma-1)M_0^2\left(f+\frac{UV^2}{\xi}\right)$$

Or

$$\frac{d}{d\xi}\left(\xi\frac{d\Theta}{d\xi}\right)-\Pr U\xi\frac{d\Theta}{d\xi}+\Pr(\gamma-1)M_0^2\left(f\xi+UV^2\right)=0$$

The boundary conditions for solving the energy equation for temperature are:

(I) $\xi=0;\qquad \frac{d\Theta}{d\xi}=0$

(II) *when* $\xi\to\infty,\quad \Theta\to 1$

Now, let $Y=\xi\frac{d\Theta}{d\xi}$

Therefore,

$$\frac{dY}{d\xi}-\Pr UY=-\Pr(\gamma-1)M_0^2\left(f\xi+UV^2\right)$$

Integrating factor (λ) used for solving above equation is given as

$$\lambda=\exp\left(-\int\Pr U\,d\xi\right)$$

The energy equation becomes

$$d(Y\lambda)=-\Pr(\gamma-1)M_0^2\left(f\xi+UV^2\right)\lambda d\xi$$

Integrating above equation with limits from vortex center to point on vortex periphery, equation becomes

$$\int_0^{\xi} d(Y\lambda) = -\Pr(\gamma-1)M_0^2 \int_0^{\xi} \left(f\xi + UV^2\right)\lambda\, d\xi$$

$$\xi\lambda\frac{d\Theta}{d\xi} - \left(\xi\lambda\frac{d\Theta}{d\xi}\right)_{\xi=0} = -\Pr(\gamma-1)M_0^2 \int_0^{\xi} \left(f\xi + UV^2\right)\lambda\, d\xi$$

Since $\left(\xi\lambda\frac{d\Theta}{d\xi}\right)_{\xi=0}$ =0

Above equation becomes

$$\xi\lambda\frac{d\Theta}{d\xi} = -\Pr(\gamma-1)M_0^2 \int_0^{\xi} \left(f\xi + UV^2\right)\lambda\, d\xi$$

Or $$\frac{d\Theta}{d\xi} = -\Pr(\gamma-1)M_0^2 \frac{\int_0^{\xi} \left(f\xi + UV^2\right)\lambda\, d\xi}{\xi\lambda}$$

Integrating again with ξ, equation becomes

$$\Theta = -\Pr(\gamma-1)M_0^2 \int_0^{\xi} \left\{\frac{\int_0^{\xi} \left(f\xi + UV^2\right)\lambda\, d\xi}{\xi\lambda}\right\} d\xi + \Theta_{\xi=0}$$

Using second boundary condition and taking ξ as infinity, equation gives

$$\Theta_{\xi\to\infty} = -\Pr(\gamma-1)M_0^2 \int_0^{\infty} \left\{\frac{\int_0^{\xi} \left(f\xi + UV^2\right)\lambda\, d\xi}{\xi\lambda}\right\} d\xi + \Theta_{\xi=0}$$

As we know from second boundary condition that

$$\Theta_{\xi\to\infty} = 1$$

Therefore, it gives

$$\Theta_{\xi=0} = 1 + \Pr(\gamma - 1) M_0^2 \int_0^{\infty} \left\{ \frac{\int_0^{\xi} \left(f\xi + UV^2 \right) \lambda \, d\xi}{\xi\lambda} \right\} d\xi$$

$$\Theta_{\xi=0} = -\Pr(\gamma - 1) M_0^2 \int_0^{\xi} \left\{ \frac{\int_0^{\xi} \left(f\xi + UV^2 \right) \lambda \, d\xi}{\xi\lambda} \right\} d\xi + 1 + \Pr(\gamma - 1) M_0^2 \int_0^{\infty} \left\{ \frac{\int_0^{\xi} \left(f\xi + UV^2 \right) \lambda \, d\xi}{\xi\lambda} \right\} d\xi$$

which gives the value of Θ in radial direction.

For this thesis case, the relation used for V,U, f and λ are given below:

$$V = (\beta + 1)^m \frac{\xi}{\left(\beta + \xi^4 \right)^m} \quad where \quad m = \frac{\beta + 1}{4}$$

$$U = \frac{\dfrac{d}{d\xi}\left(\dfrac{1}{\xi} \dfrac{d}{d\xi} (V\xi) \right)}{\dfrac{1}{\xi} \dfrac{d}{d\xi} (V\xi)}$$

$$U = -\left(\frac{4ma\xi^7}{a\xi^8 + b\xi^4 + c} + \frac{12\beta m \xi^3}{a\xi^8 + b\xi^4 + c} \right)$$

$$a = -(2m - 1), \quad b = -2\beta(m - 1), \quad c = \beta^2$$

Where

$$f = \xi^2 \left\{ \frac{d}{d\xi} \left[\frac{V}{\xi} \right] \right\}^2$$

$$f = \frac{16m^2 (\beta + 1)^{2m} \xi^8}{\left(\beta + \xi^4 \right)^{2(m+1)}}$$

$$\lambda = \exp\left(-\int \Pr U \, d\xi \right)$$

$$\lambda = \left[\frac{2a\xi^4 + b - \sqrt{\beta^2 - 4ac}}{2a\xi^4 + b + \sqrt{\beta^2 - 4ac}}\right]^{\frac{3\beta m \Pr}{\sqrt{\beta^2 - 4ac}}} \left[\frac{\left(a\xi^8 + b\xi^4 + c\right)^{\frac{1}{2a}}}{\left\{\frac{2a\xi^4 + b - \sqrt{\beta^2 - 4ac}}{2a\xi^4 + b + \sqrt{\beta^2 - 4ac}}\right\}^{\frac{b}{2a\sqrt{\beta^2 - 4ac}}}}\right]^{ma\Pr}$$

Appendix B

The source code for solving the equation in MATLAB

I. For turbulent case

```
% All properties(constant) values at different MACH numbers i.e.
% Temperature, pressure and Density

clc;
clear all;
close all;
format long;

Beta=0.7;
m=(Beta+1)/4;
Pr = 2/3;
k=1.4;
Mach=0.8;

a = -((2.*m)-1);
b = -2.*Beta.*(m-1);
c = Beta.^2;

lambda = @(x) (((2.*a.*x.^4 + b- (b.^2-4.*a.*c).^(0.5))./(2.*a.*x.^4+ b
+(b.^2-4.*a.*c).^(0.5))).^((3.*Beta.*m.*Pr)./((b.^2-
4.*a.*c).^(0.5))).*((((a.*x.^8 + b.*x.^4 + c).^(0.5)./((2.*a.*x.^4 + b-
(b.^2-4.*a.*c).^(0.5))./(2.*a.*x.^4+ b +(b.^2-
4.*a.*c).^(0.5))).^(b./(2.*(b.^2-4.*a.*c).^(0.5)))))).^(m.*Pr));
u =@(x) -
((4.*m.*a.*x.^7)./(a.*x.^8+b.*x.^4+c)+(12.*Beta.*m.*x.^3)./(a.*x.^8+b.*x.^4+c
));
v= @(x) (x.*(Beta+1).^m)./(Beta+x.^4).^m;
f =@(x) (16.*m.^2.*(Beta+1).^(2.*m).*(x.^8))./((Beta+x.^4).^(2.*(m+1)));
g = @(x) (x.*f(x)+(u(x).*v(x).^2)).*lambda(x);

h=0.001;
n= 200;
sum=zeros(1,1);

for i=h:h:n;
    x=(i-h/2);
    G=quadl(g,0,x);

    K=@(x) G./((x).*lambda(x));
    sum= sum+(h*K(x));

end
theta_zero= (sum*0.4*(2/3).*Mach.^2)+1;
```

```
sum1=zeros(1,1);
theta_z=zeros(n/h,1);
theta=zeros(n/h,1);
T1=zeros(n/h,1);

for L=1:1:(n/h)
    j=(L*h);
    i=(j-h/2);
    G1=quadl(g,0,i);

    K1=@(i) G1./(i.*lambda(i));

    sum1 = sum1+(h*K1(i));

    T1(L)= (sum1.*0.4.*(2./3).*Mach.^2);

    theta_z(L) = theta_zero;
    theta(L) = theta_z(L)-T1(L) ;

end

D1=zeros(1,1);
D2=zeros(n/h,1);
D3=zeros(1,1);
D_zero=zeros(1,1);
D=zeros(n/h,1);

for i=1:1:n/h
    j1=i*h;
    x=(i-1/2)*h;

    DENSITY=@(x) (x.*((Beta+1)./(Beta+x.^4)).^(2.*m));

     D1=quadl(DENSITY,0,n);
     D2(i)=quadl(DENSITY,0,j1);

    D3=(D1.*k.*Mach.^2)/theta_zero;
    D_zero=(exp(-D3)/theta_zero);

    D(i)=(1/theta(i))*(exp(k.*(Mach.^2).*(D2(i)-(D1))./theta(i)));
end

lam = 5;
delta=zeros(n/h,1);
intensity = zeros(n/h,1);

D(n/h +1)=1;
D(n/h +2) =1;
delta_isen=zeros(n/h,1);
inten_isentropic=zeros(n/h,1);

for i=2:1:n/h
    x=(i-1/2)*h;
    delta_isen(i) =  ((Mach.^2.*(2.*(1-x.^4).*theta(i) + (2-
k).*Mach.^2.*x.^2).*theta(i).^((3-2.*k)/(k-1)))./(1+x.^4).^2);
```

```
    delta(i) = (D(i+1)- D(i-1))./(2*h*i) + (D(i-1) + D(i+1) -2*D(i))./(h.^2)
;
  inten_isentropic(i) = 1./abs(1+ lam.*delta_isen(i));
  intensity(i) = 1./abs(1+ lam.*delta(i));
end
intensity_firstpt = (D(2)-D(1))/h + (D(1) + D(3) - 2*D(1))/h^2;
intensity_zero = (D(1)-D_zero)/h + (D_zero - 2*D(1) + D(2) )/h^2;
```

II. For Laminar case

```
%All properties(constant) values at different MACH numbers i.e.
% Temperature, pressure and Density

clc;
clear all;
close all;
format long;


Pr = 2/3;
k=1.4;
Mach=0.6;
lam = 5;


u =@(x) -(6.*x.^3./(1+x.^4));
v= @(x) (x./(1 + x.^4).^(1/2));
f = @(x) 4.*x.^8./((1 + x.^4).^3);

lambda = @(x) (1 + x.^4);

g = @(x) (x.*f(x)+(u(x).*v(x).^2)).*lambda(x);


h=0.001;
n= 200;
sum=zeros(1,1);

for i=h:h:n;
    x=(i-h/2);
    G=quadl(g,0,x);

    K=@(x) G./((x).*lambda(x));
    sum= sum+(h*K(x));

end
theta_zero= (sum*0.4*(2/3).*Mach.^2)+1;

sum1=zeros(1,1);
theta_z=zeros(n/h,1);
theta=zeros(n/h,1);
T1=zeros(n/h,1);

for L=1:1:(n/h)
    j=(L*h);
    i=(j-h/2);
    G1=quadl(g,0,i);

    K1=@(i) G1./(i.*lambda(i));
```

```
    sum1 = sum1+(h*K1(i));

    T1(L)= (sum1.*(k-1).*Pr.*Mach.^2);

    theta_z(L) = theta_zero;
    theta(L) = theta_z(L)-T1(L) ;

end

D1=zeros(1,1);
D2=zeros(n/h,1);
D3=zeros(1,1);
D_zero=zeros(1,1);
D=zeros(n/h,1);

for i=1:1:n/h
    j1=i*h;
    x=(i-1/2)*h;

    DENSITY=@(x) (x./(1 +x.^4));

     D1=quadl(DENSITY,0,n);
     D2(i)=quadl(DENSITY,0,j1);

    D3=(D1.*k.*Mach.^2)/theta_zero;
    D_zero=(exp(-D3)/theta_zero);

    D(i)=(1/theta(i))*(exp(k.*(Mach.^2).*(D2(i)-(D1))./theta(i)));
end

p_zero=D_zero*theta_zero;

p=zeros(n/h,1);


for i=1:1:n/h
   p(i)=D(i)*theta(i);
end



delta=zeros(n/h,1);
intensity = zeros(n/h,1);

D(n/h +1)=1;

for i=2:1:n/h
    x = (i-1/2)*h;


   delta(i) = (D(i+1)- D(i-1))./(2*h*x) + (D(i-1) + D(i+1) -2*D(i))./(h.^2) ;


     intensity(i) = 1./abs(1+ lam.*delta(i));
```

```
end
delta_firstpt = (D(2)-D_zero)/(h*0.0005) + (D_zero + D(2) - 2*D(1))/h^2;

delta_zero = (D(1)-D_zero)/(h*0.0005) + (D_zero - 2*D(1) + D(2) )/h^2;

intensity_firstpt = 1./abs(1+ lam.*delta_firstpt);

intensity_zero = 1./abs(1+ lam.*delta_zero);
```